Molecular Genetics and Metabolism xxx (xxxx) xxx

Contents lists available at ScienceDirect

Molecular Genetics and Metabolism

journal homepage: www.elsevier.com/locate/ymgme

Regular Article

The first knock-in rat model for glutaric aciduria type I allows further insights into pathophysiology in brain and periphery

Mary Gonzalez Melo [a], Noémie Remacle [a], Hong-Phuc Cudré-Cung [a], Clothilde Roux [b], Martin Poms [c], Cristina Cudalbu [d,e], Madalena Barroso [f], Søren Waldemar Gersting [f], René Günther Feichtinger [g], Johannes Adalbert Mayr [g], Michele Costanzo [h,i], Marianna Caterino [h,i], Margherita Ruoppolo [h,i], Véronique Rüfenacht [j], Johannes Häberle [j], Olivier Braissant [b], Diana Ballhausen [a,*]

[a] Pediatric Metabolic Unit, Pediatrics, Woman-Mother-Child Department, University of Lausanne and University Hospital of Lausanne, Switzerland
[b] Service of Clinical Chemistry, University of Lausanne and University Hospital of Lausanne, Switzerland
[c] Klinische Chemie und Biochemie Universitäts-Kinderspital Zürich, Switzerland
[d] CIBM Center for Biomedical Imaging, Switzerland
[e] Animal Imaging and Technology, Ecole Polytechnique Fédérale de Lausanne, Lausanne, Switzerland
[f] University Children's Research, UCR@Kinder-UKE, University Medical Center Hamburg-Eppendorf, Hamburg, Germany
[g] Department of Pediatrics, University Hospital Salzburg, Paracelsus Medical University, Salzburg, Austria
[h] Department of Molecular Medicine and Medical Biotechnology, School of Medicine, University of Naples Federico II, 80131 Naples, Italy
[i] CEINGE – Biotecnologie Avanzate s.c.ar.l., 80145 Naples, Italy
[j] Division of Metabolism and Children's Research Center, University Children's Hospital Zurich, Zurich, Switzerland

ARTICLE INFO

Article history:
Received 4 February 2021
Received in revised form 10 March 2021
Accepted 30 March 2021
Available online xxxx

Keywords:
Glutaric aciduria type I
Cerebral organic aciduria
Lysine degradation
Hyperammonemia
Astrogliosis
Microglial activation

ABSTRACT

Glutaric aciduria type I (GA-I, OMIM # 231670) is an inborn error of metabolism caused by a deficiency of glutaryl-CoA dehydrogenase (GCDH). Patients develop acute encephalopathic crises (AEC) with striatal injury most often triggered by catabolic stress. The pathophysiology of GA-I, particularly in brain, is still not fully understood.

We generated the first knock-in rat model for GA-I by introduction of the mutation p.R411W, the rat sequence homologue of the most common Caucasian mutation p.R402W, into the *Gcdh* gene of Sprague Dawley rats by CRISPR/Cas9 technology. Homozygous $Gcdh^{ki/ki}$ rats revealed a high excretor phenotype, but did not present any signs of AEC under normal diet (ND). Exposure to a high lysine diet (HLD, 4.7%) after weaning resulted in clinical and biochemical signs of AEC.

A significant increase of plasmatic ammonium concentrations was found in $Gcdh^{ki/ki}$ rats under HLD, accompanied by a decrease of urea concentrations and a concomitant increase of arginine excretion. This might indicate an inhibition of the urea cycle. $Gcdh^{ki/ki}$ rats exposed to HLD showed highly diminished food intake resulting in severely decreased weight gain and moderate reduction of body mass index (BMI). This constellation suggests a loss of appetite. Under HLD, pipecolic acid increased significantly in cerebral and extra-cerebral liquids and tissues of $Gcdh^{ki/ki}$ rats, but not in WT rats. It seems that $Gcdh^{ki/ki}$ rats under HLD activate the pipecolate pathway for lysine degradation. $Gcdh^{ki/ki}$ rat brains revealed depletion of free carnitine, microglial activation, astroglyosis, astrocytic death by apoptosis, increased vacuole numbers, impaired OXPHOS activities and neuronal damage.

Abbreviations: AAA, α- aminoadipic acid; AASA, α- aminoadipic semialdehyde; AASS, α- aminoadipic semialdehyde synthase; Ala, alanine; Arg, arginine; Asc, ascorbate; AEC, acute encephalopathic crisis; BMI, body mass index; Cr, creatine; CNS, central nervous system; CPS1, Carbamoyl phosphate synthetase 1; CS, citrate synthase; C0, Free carnitine; C5DC, glutarylcarnitine; FA, formic acid; GA-I, glutaric aciduria type I; GA, glutaric acid; GABA, γ-aminobutyrate; GCDH, Glutaryl CoA dehydrogenase; GFAP, Glial Fibrillary Acidic Protein; GL, granular layer; Gln, glutamine; Glu, glutamate; GPC, glycerophosphocholine; GSH, glutathione; HE, hematoxylin and eosin; HLD, high lysine diet; HRMS/MS, high-resolution tandem mass spectrometry; Iba1, Ionized calcium binding adaptor molecule 1; Ins, myo-inositol; KI, Knock-in; Lac, lactate; Lys, lysine; MAP2, Microtubule-associated protein 2; ML, molecular layer; NAA, *N*-acetylaspartate; ND, normal diet; Ndufs4, NADH dehydrogenase [ubiquinone] iron-sulfur protein 4; Ndufs6, NADH dehydrogenase [ubiquinone] iron-sulfur protein 6; NH_4^+, ammonium; Orn, ornithine; PE, phosphoethanolamine; PC6, piperideine 6-carboxylate; PCr, phosphocreatine; PL, Purkinje layer; SD, Sprague Dawley; Tau, taurine; UHPLC, ultra-high performance liquid chromatography; WT, wild type; WM, white matter; 1H-MRS, proton magnetic resonance spectroscopy; 2AAA, 2-aminoadipic acid; 3-OHGA, 3-hydroxyglutaric acid.

* Corresponding author at: Unité pédiatrique des maladies métaboliques, Service de Pédiatrie, Département Femme-Mère-Enfant, Centre Hospitalier Universitaire Vaudois, CHUV MP18-05/565, Chemin du Mont-Paisible 18, CH-1011 Lausanne, Switzerland.

E-mail addresses: mary.gonzalez-melo@chuv.chm (M. Gonzalez Melo), Clothilde.Roux@chuv.ch (C. Roux), Martin.Poms@kispi.uzh.ch (M. Poms), cristina.cudalbu@epfl.ch (C. Cudalbu), m.barroso@uke.de (M. Barroso), gersting@uke.de (S.W. Gersting), r.feichtinger@salk.at (R.G. Feichtinger), h.Mayr@salk.at (J.A. Mayr), michele.costanzo@unina.it (M. Costanzo), marianna.caterino@unina.it (M. Caterino), margherita.ruoppolo@unina.it (M. Ruoppolo), veronique.ruefenacht@kispi.uzh.ch (V. Rüfenacht), Johannes.Haeberle@kispi.uzh.ch (J. Häberle), Olivier.Braissant@chuv.ch (O. Braissant), diana.ballhausen@chuv.ch (D. Ballhausen).

https://doi.org/10.1016/j.ymgme.2021.03.017

Under HLD, *Gcdh*$^{ki/ki}$ rats showed imbalance of intra- and extracellular creatine concentrations and indirect signs of an intracerebral ammonium accumulation.
We successfully created the first rat model for GA-I. Characterization of this *Gcdh*$^{ki/ki}$ strain confirmed that it is a suitable model not only for the study of pathophysiological processes, but also for the development of new therapeutic interventions. We further brought up interesting new insights into the pathophysiology of GA-I in brain and periphery.

1. Introduction

Glutaryl-CoA dehydrogenase (EC 1.3.8.6; GCDH) is a nuclear-encoded homotetrameric mitochondrial flavoprotein belonging to the acyl-CoA dehydrogenase family. It is involved in the catabolic pathway of tryptophan, lysine and hydroxylysine and catalyzes the dehydrogenation and decarboxylation of glutaryl-CoA to crotonyl-CoA and carbon dioxide. Glutaric aciduria type I (GA-I), due to GCDH deficiency, is characterized by the accumulation of glutaryl-CoA and its dicarboxylic derivatives, namely glutaric acid (GA), 3-hydroxyglutaric acid (3OHGA), glutaconic acid, and glutarylcarnitine (C5DC) in body fluids and tissues [1–3]. So far, two pathways of lysine degradation have been described: saccharopine (ε-deamination of lysine) and pipecolic acid (α-deamination of lysine) pathways, both converging in mitochondria into a common pathway at 2-aminoadipic acid (2AAA). Based on radiolabeling studies performed in rat and mouse it was a long time believed that lysine degradation is different in adult mammalian brain and extracerebral tissues [4–6]. The saccharopine pathway was thought to be the predominant lysine degradation pathway in extra-cerebral tissues, while the pipecolic acid pathway appeared to be predominant in the adult brain [6]. However, recent studies revealed that the saccharopine pathway is also predominant in human brain cells and that both pathways seem to be active in mouse brain [7–11].

The estimated prevalence of GA-I is about 1:100′000 worldwide [3]. Patients with GA-I develop macrocephaly with frontotemporal cortical atrophy. GA-I was until very recently thought to manifest exclusively with neurologic symptoms and therefore is classified as a cerebral organic aciduria [12]. Alterations of brain development are known to start already before birth [13–15]. Development of often transient truncal hypotonia and delayed motor development have been observed in about 50% of GA-I patients during the first year of life [16]. Development of macrocephaly, frontotemporal hypoplasia, signs of early vascular dysfunction in the form of subdural effusions, intradural and retinal hemorrhages as well as delayed myelination can already be present in the pre-symptomatic period [17]. If untreated, most patients present an acute encephalopathic crisis (AEC) that typically occurs between the 3rd and the 36th month of life following a catabolic state due to gastroenteritis or febrile disease. This disease presentation is called acute onset. During this crisis, extensive neuronal damage occurs, typically in caudate and putamen nuclei, resulting in an irreversible, complex, predominantly and dystonic movement disorder [3]. This sequence resembles the observations of patients suffering from ischemic stroke. Acute restricted diffusion is a typical sign of cytotoxic edema. The risk for an AEC significantly diminishes beyond the age of 2 years. It seems that the vulnerability of the striatum decreases with age. Even without AEC, patients can show subtle but significant fine motor and speech deficits that witness chronic neurological damage [18] or even develop a movement disorder. This presentation is called insidious onset. In these patients, MRI studies revealed more circumscribed T2-hyperintensities of the dorsolateral putamen without development of atrophy in follow-up studies. Insidious onset patients showed a latency phase between the detection of striatal lesions on MRIs and the onset of clinical dystonia. It seems that striatal injury first affects the dorsolateral putamen and that the severity of the resulting dystonia is dependent on the extension of the striatal lesion [19]. Deviations from the normal treatment, in particular an appropriate and immediate emergency management, have been identified to be the major risk factor for the development of an insidious onset form even after diagnosis by newborn screening [3,16]. Interestingly, patients with late diagnosis of GA-I (called late-onset) all show a high excretor phenotype [20]. In contrast to the observations on the striatal region in GA-I patients there is growing evidence that extra-striatal changes, particularly in the white matter, are progressive with age and develop despite early diagnosis through newborn screening and presymptomatic treatment [21].

Different animal models of GA-I have been created to contribute to understand the pathomechanisms responsible for neurodegeneration. A *Gcdh*$^{-/-}$ mouse was developed by Koeller et al. via homologous insertion of a gene-targeting vector, which resulted in deletion of the first seven exons of the *Gcdh* gene [22]. This model presents high levels of GA and 3-OHGA as in the majority of patients. Under high lysine or high protein overload, this GA-I mouse model presents disruption of redox and bioenergetics homeostasis, neuroinflammation, disturbance of glutamatergic and GABAergic neurotransmission, vascular abnormalities, myelopathy, as well as striatum and cortex damage [1,23–26].

More than 150 mutations in the *GCDH* gene have been described in GA-I patients [27]. The most common mutation in the Caucasian population is p.R402W [28,29]. This mutation is associated with a residual enzymatic activity of 0–5% in patient fibroblasts, and characterized with a high excretion of GA and 3-OHGA in urine [30]. As rat models are more and more recognized as superior to mice for the study human brain pathologies [31], we decided to introduce the mutation p.R411W, the rat homologue of the human p.R402W mutation, into Sprague-Dawley rats by CRISPR/Cas9 technology.

2. Materials and methods

2.1. Ethics statement

This study was carried out in strict accordance with the ethical principles and guidelines for scientific experiments on animals of the Swiss Academy for the Medical Sciences. The ethics committee for animal experimentation for the canton of Vaud (authorization VD2967) approved the protocols. Animals were kept in single ventilated cages and under controlled humidity and temperature (21–23 °C), on 12 h/12 h day/night cycle. Whenever possible, littermate controls were used to compare experimental groups.

2.2. Creation of the *Gcdh*$^{ki/ki}$ rat model

The rat *Gcdh* gene contains 12 exons with the ATG start codon in exon 2 and TGA stop codon in exon 12. It is localized on chromosome 19q11, within a region of high homology to the human chromosome 19. The mutation p.R402W is the most frequent *GCDH* mutation in Caucasians and results in GA-I with a high excretor phenotype. The rat *Gcdh* mutation p.R411W, which based on sequence homology corresponds to the *GCDH* mutation p.R402W, was introduced into Sprague-Dawley rats by CRISPR/Cas9 technology (Cyagen, Fig. 1A). Genotyping was performed on genomic DNA from ear biopsies using the KAPA BIOSYSTEMS kit (ref. KK7352) and the following primers for PCR amplification (QIAGEN kit ref. 201,445, Fig. 1B):

F: 5'-AGGCGTATGCTACCACTGCTCAG-3′
R: 5'-TCAGGAGCATCTCACAGGGTCAT-3′

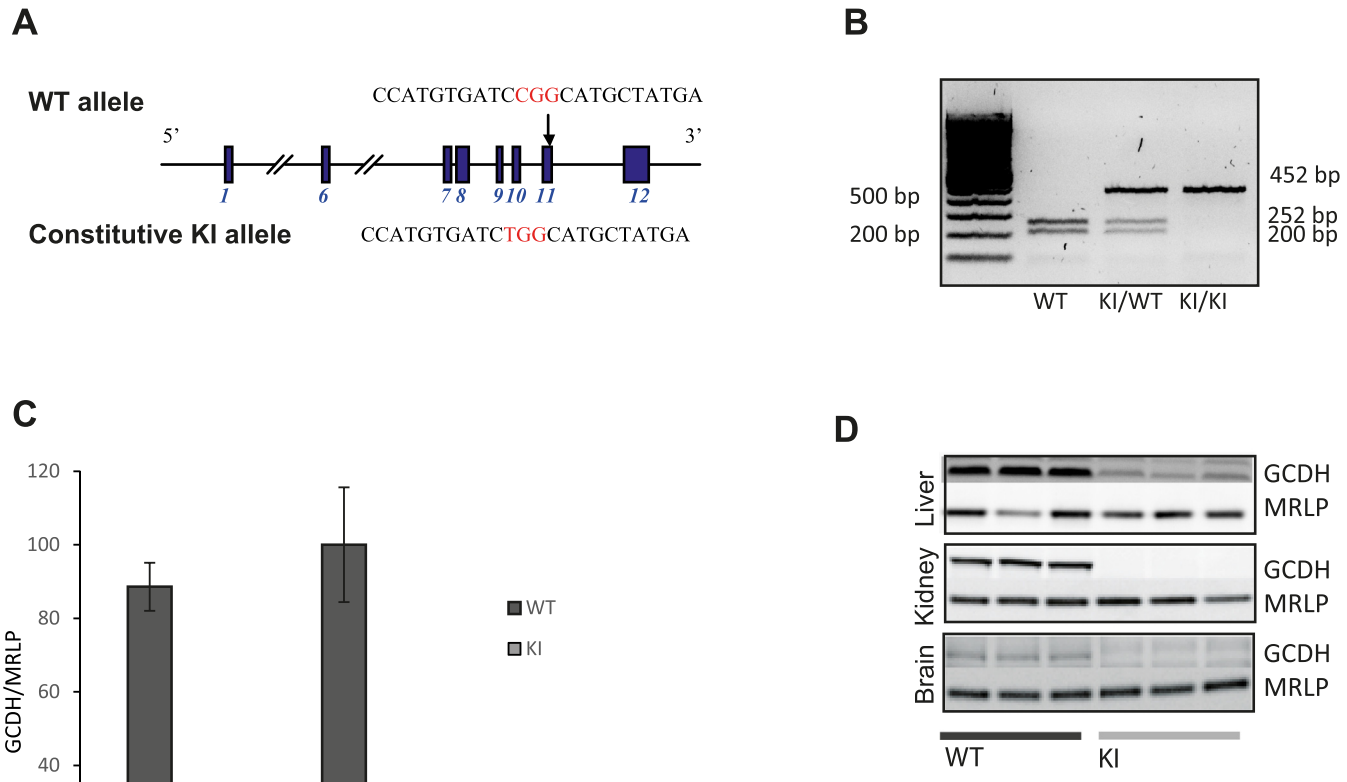
A
WT allele
CCATGTGATCCGGCATGCTATGA
5'
3'
1
6
7 8
9 10
11
12
Constitutive KI allele
CCATGTGATCTGGCATGCTATGA
B
500 bp
200 bp
452 bp
252 bp
200 bp
WT
KI/WT
KI/KI
C
GCDH/MRLP
120
100
80
60
40
20
0
WT
KI
Liver
Kidney
Brain
D
Liver
Kidney
Brain
GCDH
MRLP
WT
KI
E
Liver
Kidney
Brain
Heart
GCDH activity
[Crotonyl-CoA (pmol/min/mg)]
WT
KI
*
**

PCR conditions were as follows: 10 min 95 °C, 35× [30 s 95 °C, 1 min 56 °C, 1 min 30 s 72 °C], 10 min 72 °C, then stored at 4 °C. After PCR amplification, an enzymatic digestion with the MspI restriction enzyme (Promega, R6401, Madison USA) was performed for 4 h at 37 °C. As in *Gcdh*$^{ki/ki}$ rats the restriction site was suppressed, we obtained one single fragment of 452 bp, while the WT strain was cut in two fragments of 252 bp and 200 bp. Heterozygotes presented three bands of 452 bp, 252 bp and 200 bp (Fig. 1B). This new rat strain was named SD-Gcdh^{em1Dba}. Homozygous mutant rats were named *Gcdh*$^{ki/ki}$ (KI) rats in this manuscript.

2.3. High lysine diet

Gcdh$^{ki/ki}$ and WT rats were challenged with a high lysine diet (HLD) from the age of 3 weeks (after weaning) over 21 days (until the age of 6 weeks). For HLD, we applied a chow containing 4.7% of L-lysine (Safe diet U8978P01R) instead of 1.1% L-lysine in the normal diet (ND, Kliba Nafab 3242). 12 (6 females and 6 males) WT and 12 (6 females and 6 males) *Gcdh*$^{ki/ki}$ rats were submitted to HLD in three independent experiments. An age-matched control group of 4 (2 females and 2 males) WT and 4 (2 females and 2 males) *Gcdh*$^{ki/ki}$ rats was kept on ND. Anthropometric measures were taken once weekly, food intake was determined daily. Weight gain and BMI were calculated.

2.4. Measurement of GCDH enzymatic activity

GCDH catalyzes the oxidative decarboxylation of glutaryl-CoA to crotonyl-CoA, which is directly metabolized to 3-hydroxybutyryl-CoA in the presence of enoyl-CoA hydratase. GCDH activity in rat tissue was determined after tissue homogenization and lysis in HEPES buffer (20 mM HEPES, pH 7.0). Briefly, 0.2–0.6 mg/mL of tissue were assayed in 75 mM potassium phosphate buffer (pH 7.4), 0.075 mM flavin adenine dinucleotide (FAD), 0.3 mM ferrocenium hexafluorophosphate, and 0.01 mM glutaryl-CoA, at 37 °C. The reaction was stopped using hydrochloric acid, followed by pH neutralization with potassium hydroxide. An excess of L-cysteine was added to complete ferrocenium reduction. Separation and quantification of glutaryl-CoA, crotonyl-CoA, and 3-hydroxybutyryl-CoA were performed using reversed-phase (C18 column) HPLC with detection at 260 nm. Standards were included for all the metabolites monitored (Sigma-Aldrich). The GCDH activity (formation of pmol Crotonyl-CoA/min/mg of total protein) was calculated based on the conversion rate of crotonyl-CoA to 3-hydroxybutyryl-CoA in rat tissue lysates.

2.5. Tissue preparation

WT and *Gcdh*$^{ki/ki}$ rats at 6 weeks of age under HLD and ND were sacrificed by decapitation and immediately dissected. Different organs (brain, kidney, liver and heart) were extracted. Half of each animal tissue was frozen in liquid nitrogen to perform enzymatic assays and protein analyses (western blotting) while the other half was embedded in paraffin for histology.

2.6. Measurements of organic acids and glutarylcarnitine

Organic acids and glutarylcarnitine were measured in plasma and urine of *Gcdh*$^{ki/ki}$ and WT rats at the age of 3 weeks under ND and at 6 weeks of age under ND or after 21 days of HLD. Measurements in CSF were only performed in *Gcdh*$^{ki/ki}$ and WT rats at the age of 6 weeks under ND or HLD. All measurements were performed using a semi-quantitative ultra-high performance liquid chromatography (UHPLC) high-resolution tandem mass spectrometry (HRMS/MS) approach. Plasma samples were prepared by precipitating 30 μL of plasma with 120 μL of ice-cold methanol, centrifuged, evaporated and subsequently redissolved in 60 μL sample buffer (water, 0.1% FA). Urine samples were diluted with water to a normalized creatinine level of 0.01 mM and acidified to a final FA concentration of 0.1%. CSF samples were analyzed undiluted with the addition of formic acid to a final concentration of 0.1%.

Metabolites were separated using an ACQUITY UPLC® HSS T3 1.8 μm, 100 × 2.1 mm I.D. column (Waters, Massachusetts, US) and eluted using the following gradient from solvent A (water, 5 mM ammonium formate, 0.1% formic acid) to solvent B (methanol, 5 mM ammonium formate, 0.1% formic acid) as follows: 2 min at 0% B, 2–3.5 min to 4% B, 3.5–10 min to 45% B, 10–12 min to 70% B, 12–13.5 min to 100% B, with an isocratic plateau at 100% B for 2 min to 15.5 min, and from 15.5–16.5 min to 0% B. The column was re-equilibrated after each run for 8 min at 100% A.

Mass spectra were acquired using a heated electro-spray ionization (HESI) source of a Q-Exactive high resolution, accurate mass spectrometer (Thermo Scientific, Waltham, MS, USA). Mass spectra were recorded in positive and negative mode with the MS detector in full-scan mode (Full-MS) in the scan-range 50 to 750 *m/z* with data-dependent (dd-MS2) acquisition of fragment ions from the top-5 most abundant ions per scan.

HESI parameters: sheath gas flow rate 35 arbitrary units (AU), auxiliary gas flow rate 35 AU, sweep gas flow rate 2 AU, spray voltage 3.5 kV, capillary temperature 350 °C, aux gas heater temperature 350 °C. Detector settings for full MS: In-source CID 0.0 eV, μscans = 1, resolution = 70,000, AGC target 1e6, max IT = 35 ms, spectrum data type, profile. Detector setting for dd-MS2 were: μscans = 1, resolution = 17,500, AGC target 1e5, max IT = 80 ms, loop count = 5, isolation window 4.0 *m/z*, NCE 30.0, intensity threshold 1.3e4, apex trigger 2 to 4 s, spectrum data type, profile.

Peaks were integrated with Xcalibur (version 4.0.27.19, Thermo Fisher Scientific) using windows of 0.01 *m/z* and 20 s for retention time and subsequently normalized using isotopically labelled internal standards.

The measurements of organic acids and glutarylcarnitine in striatum tissue of 6-week-old *Gcdh*$^{ki/ki}$ and WT rats under ND or HLD were performed as described previously [32].

2.7. Quantification of amino acids and NH_4^+

NH_4^+ was measured on an Integra automatic analyzer (Roche) as described previously [32]. Amino acids were measured in plasma of 6-week-old *Gcdh*$^{ki/ki}$ and WT rats under ND or HLD. The samples were analyzed by LC-MS on a Waters QDa single quadrupole mass spectrometer coupled with a H-class UPLC system. After a protein precipitation step with the addition of 10% m/v sulfosalicylic acid solution containing 20 ^{13}C and for most of them also ^{15}N isotopically labelled amino acids as internal standards, free amino acids were derivatized according to a modified protocol of the Waters Corp. AccQ•Tag™ derivatization kit. Modified amino acids were separated using a Cortex UPLC C18 (1.6

Fig. 1. Generation of the knock-in *Gcdh* rat allele and initial characterization of *Gcdh*$^{ki/ki}$ (KI) rats. (**A**) Based on the sequence of the WT rat *Gcdh* gene, a targeting construct was generated by Crispr/CAS9 technology in order to insert the missense mutation p.R411W, which corresponds to the frequent Caucasian *GCDH* mutation p.R402W. (**B**) For genotyping, genomic DNA was extracted from ear biopsies. Exon 11 of the *Gcdh* gene was amplified by PCR, digested with the restriction enzyme *Msp*I (cuts the WT sequence, but not the mutated sequence) and migrated on an agarose gel. Wild type (WT) rats were recognized by presence of two bands (252 bp and 200 bp), *Gcdh*$^{ki/wt}$ rats by three bands (452 bp, 252 bp and 200 bp) and *Gcdh*$^{ki/ki}$ (KI) rats by one band (452 bp). (**C**) Quantification of GCDH protein expression by western blotting in kidney, liver and brain in 6-week-old WT and *Gcdh*$^{ki/ki}$ (KI) rats ($n = 4$). (**D**) Western blot for GCDH protein expression using MRLP as a loading control. The three first lanes correspond to WT rats and the last three to *Gcdh*$^{ki/ki}$ (KI) rats. (**E**) Enzyme activity of GCDH in brain, heart, kidney and liver of 6-week-old WT and *Gcdh*$^{ki/ki}$ (KI) rats ($n = 4$). As expected, GCDH activity was found significantly decreased in heart, kidney and liver of *Gcdh*$^{ki/ki}$ rats. No significant difference between WT and *Gcdh*$^{ki/ki}$ (KI) rats was observed in brain, which revealed a very low GCDH activity.

μm particle size, 2.1 × 150 mm) column (Waters corp.), maintained at 55 °C, with a 0.1% formic acid containing Water:Acetonitrile mobile phase gradient of 12 min. The chosen flow rate had a value of 500 μL/min and the sample injection volume was 2 μL.

Amino acids and derivatives were quantified using standard calibration curves and isotopic labelled internal standards. LC-MS data were processed using TargetLynx (Waters Corp.).

Plasma NH_4^+ was measured on an Integra automatic analyzer (Roche, Switzerland).

Amino acids measurements in urine of WT and *Gcdh*$^{ki/ki}$ rats at 6 weeks of age under HLD and ND were carried out with the same semi-quantitative method described above for organic acid measurements.

Intracellular concentrations of amino acids were measured in striatum of WT and *Gcdh*$^{ki/ki}$ rats at 6 weeks of age under HLD and ND as described before [32,33].

2.8. CPS1 enzyme activity measurements in rat liver

Carbamoyl phosphate synthetase 1 (CPS1) activity of 6-week-old *Gcdh*$^{ki/ki}$ and WT rat liver lysates was measured in triplicates using the previously described assay [34] converting carbamoyl phosphate to citrulline. In brief, liver lysates were incubated for 10 min at 37 °C in an assay mixture containing 50 mM glycyl-glycine pH 7.4, 70 mM KCl, 1 mM DTT, 20 mM $MgSO_4$, 5 mM ATP, 35 mM NH_4Cl, 50 mM $KHCO_3$, 10 mM NAG, 5 mM L-ornithine and 4 U/mL OTC. Absorbance at 464 nm was measured to calculate to amount of converted citrulline. Protein concentration was determined by the Bradford method using BSA as standard.

2.9. Proton magnetic resonance spectroscopy (1H-MRS) of CNS at high magnetic field (9.4 T)

For 1H-MRS, WT and *Gcdh*$^{ki/ki}$ rats at 6 weeks of age under HLD and ND ($n = 5$ WT rats and $n = 5$ *Gcdh*$^{ki/ki}$ rats per condition) were anesthetized with isoflurane (2% for maintenance, 70% compressed air and 30% O_2) as described [35]. In vivo 1H-MRS was performed on a horizontal actively shielded 9.4 Tesla system (Magnex Scientific, Oxford, UK) interfaced to a Varian Direct Drive console (Palo Alto, USA) using a home built 1H-quadrature surface coil (14 mm diameter) as transceiver placed over the head of the animal. The volume of interest (VOI) was positioned in striatum ($2.5 \times 2 \times 2.5$ mm^3) based on axial and sagittal anatomical T_2 weighted images (multislice turbo-spin-echo sequence, repetition time TR = 4 s, effective echo time TEeff = 52 ms, echo train length = 8, field of view = 23×23 mm^2, slice thickness = 1 mm, 2 averages, 256×256 image matrix). Localized spectra were acquired with SPECIAL spectroscopy sequence (TE = 2.8 ms, TR = 4 s, 240 averages) to obtain the specific neurochemical profile in the mentioned VOI [35,36]. Metabolite concentrations were estimated using the LCModel software as described previously [35,37].

2.10. Histology

The brain of each rat was fixed in a buffered formaldehyde solution for 24 h. Each brain was paraffin-embedded with a Leica ASP300S tissue processor (Leica, Heerbrug, Switzerland), and 3 μm tissue sagittal sections prepared with a Microm HM 335 E microtome (Thermo Scientific, Walldorf, Germany). Each section was stained with hematoxylin and eosin (HE), mounted on glass slides, and examined with a Zeiss axioscan Z.1 microscope (Zeiss, Lausanne, Switzerland) using bright field optics at 20× and 40× magnification. On digital images of representative sections, the vacuoles were quantified with Zen blue 2.6 software. In addition, brain sagittal sections from 6-week-old *Gcdh*$^{ki/ki}$ and WT rats under ND and HLD were stained with Luxol fast blue in order to search for demyelination processed and PAS staining to detect glycogen deposits.

ImmunohistochemistryFor double immunofluorescence staining the following antibodies were used: Glial Fibrillary Acidic Protein (GFAP) (1:200, Merck Millipore, MAB360), Ionized calcium binding adaptor molecule 1 (IBA1) (1:200, Abcam, ab5076; 1:100, Merck Millipore, MAB5254), Cleaved caspase 3 (Asp175) (1:100, Cell signaling) and Microtubule-associated protein 2 (MAP2) (1:100, Cell signaling, 4542). All primary antibodies were diluted in blocking buffer (1.5% donkey serum in PBS and 1× BSA-PBS; Sigma-Aldrich, Germany). The following secondary antibodies were used: anti-rabbit IgG Alexa Fluor 555 (1:200, Invitrogen, Eugene, Oregon, USA), anti-goat IgG Alexa Fluor 488 (1:200,. Invitrogen, Eugene, Oregon, USA) and anti-mouse IgG Alexa Fluor 488 (1:200, Invitrogen, Eugene, Oregon, USA). Secondary antibodies were diluted in phosphate-buffered saline (PBS) containing 0.5% Tween 20 (PBS-T, pH 7.4).

Brain sagittal sections from 6-week-old *Gcdh*$^{ki/ki}$ and WT rats under HLD or ND were deparaffinized. After two washes with PBS, sections were fixed 1 h in neutral-buffered 4% formalin followed by heat-induced epitope retrieval in EDTA-T buffer (1 mM EDTA, pH 8.0, 0.05% Tween 20) for 40 min at 95 °C and 20 min at room temperature. Sections were washed in deionized H_2O and equilibrated with PBS-T. Non-specific antibody binding sites were blocked with blocking buffer (1% bovine serum albumin, 3% donkey serum in PBS and 1× BSA-PBS; Sigma-Aldrich, Germany) for 1 h. Sections were incubated with primary antibodies overnight at 4 °C. Afterwards, sections were washed three times in PBS-T and incubated for 1 h with secondary antibodies. Specimens were again washed three times in PBS-T and incubated with 0.5 μg/mL 4′,6-diamidino-2-phenylindole (Sigma, St Louis, Missouri, USA) for 10 min. Slides were washed twice in distilled H_2O and mounted in Fluorescent Mounting Medium FluorSave™ (Merck Millipore, Germany). Sections were photographed using a Hamamatsu Nanozoomer S60 microscope with 40× objective allowing for multiple magnification through pixel binning. Images were analyzed with NDP. view2 software.

2.11. Measurements of OXPHOS complex activities

OXPHOS analyses were performed on brain sections of cerebellum, cortex, hippocampus and striatum of 6-week-old *Gcdh*$^{ki/ki}$ and WT rats under HLD or ND. Spectrophotometric measurements of OXPHOS enzyme and citrate synthase (CS) activities were performed as previously described [38]. Kidney and brain tissues (20–100 mg) were homogenized with a tissue disintegrator (Ultraturrax, IKA, Staufen, Germany) in extraction buffer (20 mM Tris-HCl, 250 mM sucrose, 40 mM KCl, 2 mM EGTA, pH 7.6) and finally homogenized with a motor-driven Teflon-glass homogenizer (Potter S, Braun, Melsungen, Germany). Homogenates were centrifuged at 600 xg for 10 min at 4 °C. The postnuclear supernatant (600 x g homogenate) containing the mitochondrial fraction was used for measurements of enzyme activities.

After initial recording of thiolase activity for 2 min, the citrate synthase reaction was started by addition of 0.5 mM oxaloacetate and was followed at 412 nm for 8 min. The mean unspecific thiolase activity was 2% of the CS activity. Enzyme activities of the OXPHOS complexes were determined as follows: rotenone sensitive complex I activity was measured spectrophotometrically as NADH/decylubiquinone oxidoreductase at 340 nm. The whole reaction mixture for the ATPase activity measurement was treated for 10 s with an ultra-sonifier (Bio cell disruptor 250, Branson, Vienna, Austria). Complex II activity was measured according to [39] with the following modifications: The reaction mixture contained 50 mM potassium phosphate pH 7.8, 2 mM EDTA, 0.1% BSA, 3 μM rotenone, 80 μM 2,6-dichlorophenol, 50 μM decylubiquinone, 1 μM antimycin A, 0.2 mM ATP, 0.3 mM KCN and the 600 x g homogenate. The mixture was preincubated for 10 min at 37 °C, started by addition of 10 mM succinate, and followed for 6 min at 600 nm. The reaction mixture for the measurement of the complex III activity contained 50 mM potassium phosphate buffer pH 7.8, 2 mM EDTA pH 8.6, 0.3 mM KCN, 100 μM cytochrome *c*, 200 μM reduced

decylubiquinol. The reaction was initiated by addition of the 600 x g homogenate. After 3–4 min, the reaction was inhibited by addition of 1 μM antimycin A. The antimycin A-insensitive activity was substracted from total activity to calculate the complex III activity. All spectrophotometric measurements (Uvicon 922, Kontron, Milan, Italy) were performed at 37 °C.

2.12. Proteomic analyses

Proteomic analyses were performed on whole brains of *Gcdh*$^{ki/ki}$ and WT rats under ND at the age of 3 ($n = 4$) and 6 (n = 4) weeks, and on striatal sections of 6-week-old *Gcdh*$^{ki/ki}$ and WT rats under ND (n = 4) or HLD ($n = 3$). The comparisons were performed using different quantitative proteomic approaches [40]. In detail, the comparisons between 3-week-old *Gcdh*$^{ki/ki}$ rats versus WT rats under ND and between 6-week-old *Gcdh*$^{ki/ki}$ rats versus WT rats under ND were performed by means of the spectral counting approach; the comparisons in striatum of 6-week-old *Gcdh*$^{ki/ki}$ and WT rats under ND or HLD by the label-free quantification (LFQ) method.

The proteomes of whole brains (2 at 3 weeks and 2 at 6 weeks for each condition) were extracted and separated by monodimensional SDS-PAGE according to De Pasquale et al. (2020) [41]. Protein in-gel digestion was carried out using trypsin as proteolytic enzyme. Peptide mixtures were analyzed by liquid chromatography – tandem mass spectrometry (LC-MS/MS) using a LTQ-Orbitrap XL mass spectrometer (Thermo Scientific, Bremen, Germany) and quantitative analysis was performed with the Thermo Proteome Discoverer (version 1.4.1.14) platform (Thermo Scientific, Bremen, Germany), as described [42]. Taxonomy was selected for *Rattus norvegicus*. Each sample was run twice as MS technical replicates. The fold change (FC) for each protein was calculated as the binary logarithm of the ratio of the average NSAF (Normalized Spectral Abundance Factor) values [43] of *Gcdh*$^{ki/ki}$ and WT rats. Differentially regulated proteins with a *t*-test *p-value* lower than or equal to 0.05 were selected as statistically significant.

Protein extracts from striatum were obtained by mechanical lysis [44] in RIPA buffer (Sigma-Aldrich, St. Louis, MO, USA) containing a protease inhibitor cocktail (Thermo Fisher Scientific, Waltham, MA, USA), and centrifugation at 14,000 xg for 20 min at 4 °C to collect the protein supernatant. The proteomic experiment was carried out by digestion on S-Trap columns (Protifi, Huntington, NY, USA), LC-MS/MS analysis using a Q Exactive PLUS mass spectrometer (Thermo Scientific, Waltham, MA, USA), and LFQ using MaxQuant software (version 1.5.8.3), as described [45]. Each sample was run thrice as MS technical replicates. For the LFQ, the fasta file for the proteome of *Rattus norvegicus* was downloaded from UniProt. The comparisons between *Gcdh*$^{ki/ki}$ versus WT rats under ND and between *Gcdh*$^{ki/ki}$ versus WT rats under HLD in striatum were carried out with the Perseus software version 1.6.0.7 (available at www.perseus-framework.org). The FC was determined as difference of the average log2 protein LFQ intensities of *Gcdh*$^{ki/ki}$ and WT samples. A *q-value* (with False Discovery Rate (FDR) = 1%, S0 = 0.5) was applied to determine the statistically significant proteins that varied in all conditions.

The differential datasets produced as explained above were graphically represented in form of volcano plots or heat maps generated by the GraphPad Prism 8 and Metaboanalyst 4.0 tools [46], respectively.

2.13. Bioinformatics analyses

To annotate age and diet dependent functional activities and molecular pathways influenced by GCDH protein depletion in rat brain tissues, the identified proteomic datasets were analyzed by the g:Profiler tool (https://biit.cs.ut.ee/gprofiler/gost). The g:Profiler data sources were: Gene Ontology, KEGG, Reactome and Human Phenotype Ontology. The *q-value* cutoff (FDR) was 0.05 [47].

2.14. Statistical analyses

Unless otherwise stated, results are presented as mean ± standard deviation. Data for quantitative measurements of organic acids in striatum, weight gain, BMI, food intake, ammonium concentrations in plasma, amino acid concentrations in plasma, amino acid concentrations in striatum, vacuoles quantifications, and OXPHOS enzymatic analyses were analyzed by two-way analyses of variance (ANOVA), considering the factors: 1) genotype: WT or *Gcdh*$^{ki/ki}$ 2) diet: ND or HLD; 3) interaction between genotype and diet. F values are presented when differences between groups were rated significant at $P < 0.05$. The post-hoc Tukey's and non-parametric Mann Whitney tests were performed when means from three or more groups were compared. Protein contents by western blotting, enzymatic activities of crotonyl CoA, semi-quantitative analyses of organic acids and semi-quantitative measurements of amino acids were analyzed by Student's *t*-test for unpaired samples to compare means between two different groups or non-parametric Mann Whitney tests. All statistical analyses were carried out using the SPSS Software (IBM Software, USA) and Graphpad Software (Graphpad Software, USA).

3. Results

3.1. Creation of the *Gcdh*$^{ki/ki}$ rat model

The rat *Gcdh* mutation p.R411W (CGG > TGG) c.1231C > T was generated by Crispr/CAS9 genome engineering (Fig. 1A-B). Breeding of *Gcdh*$^{ki/wt}$ rats displayed the expected Mendelian distribution of genotypes: 49% *Gcdh*$^{ki/wt}$, 29% *Gcdh*$^{ki/ki}$ and 22.5% *Gcdh*$^{wt/wt}$ average number of litters: 15 (data obtained from 133 pups of nine litters of heterozygous breeding pairs). The expected Mendelian distribution confirmed that *Gcdh*$^{ki/ki}$ rats had a normal foetal and postnatal viability. At early stages of life, *Gcdh*$^{ki/ki}$ rats were largely indistinguishable from *Gcdh*$^{ki/wt}$ and WT littermates (no significant difference in body weight, body size, fur colour and behavior). Breeding of *Gcdh*$^{ki/ki}$ rats revealed normal fertility and normal life span.Under ND, *Gcdh*$^{ki/ki}$ rats did not present any signs of AEC. Western blotting for GCDH showed a significantly diminished expression in kidney, liver and brain of *Gcdh*$^{ki/ki}$ rats compared with WT controls (Fig. 1C-D). While GCDH activity was found clearly diminished in kidney, heart, and liver of *Gcdh*$^{ki/ki}$ rats, the detectable enzymatic activity in brain tissue was low and no significant differences could be observed between *Gcdh*$^{ki/ki}$ and WT rats (Fig. 1E).

3.2. Biochemical phenotype of *Gcdh*$^{ki/ki}$ rats

As expected, *Gcdh*$^{ki/ki}$ rats under ND revealed a high excretor phenotype, including increase of C5DC, GA and 3-OHGA in plasma and urine at the age of 3 and 6 weeks (Fig. 2A-C). After 21 days of HLD at the age of 6 weeks, C5DC was found significantly increased in urine, CSF and striatum of *Gcdh*$^{ki/ki}$ rats, while no significant difference was observed in plasma (Fig. 2A). GA concentrations in plasma, urine and striatum increased significantly in *Gcdh*$^{ki/ki}$ rats under HLD, but no difference was observed in CSF (Fig. 2B). 3OHGA concentrations increased significantly in plasma and striatum of *Gcdh*$^{ki/ki}$ rats exposed to HLD (Fig. 2C). Free carnitine (C0) concentrations decreased in urine of *Gcdh*$^{ki/ki}$ rats under ND and in striatum of *Gcdh*$^{ki/ki}$ rats independently of the diet (Fig. 2D), while no significant difference was found in plasma and CSF.

3.3. Low food intake, slowing of weight gain and decline of BMI in *Gcdh*$^{ki/ki}$ rats under HLD

No significant differences between WT and *Gcdh*$^{ki/ki}$ rats were observed in food intake, weight gain, seize and body mass index (BMI) under ND (Fig. 3A, C, E, G and H). Under HLD, *Gcdh*$^{ki/ki}$ rats showed a severely diminished food intake ($P = 0.023$; Fig. 3 B) resulting in a significant decrease of weight gain in both genders (Fig. 3D and F; $P = 0.0015$

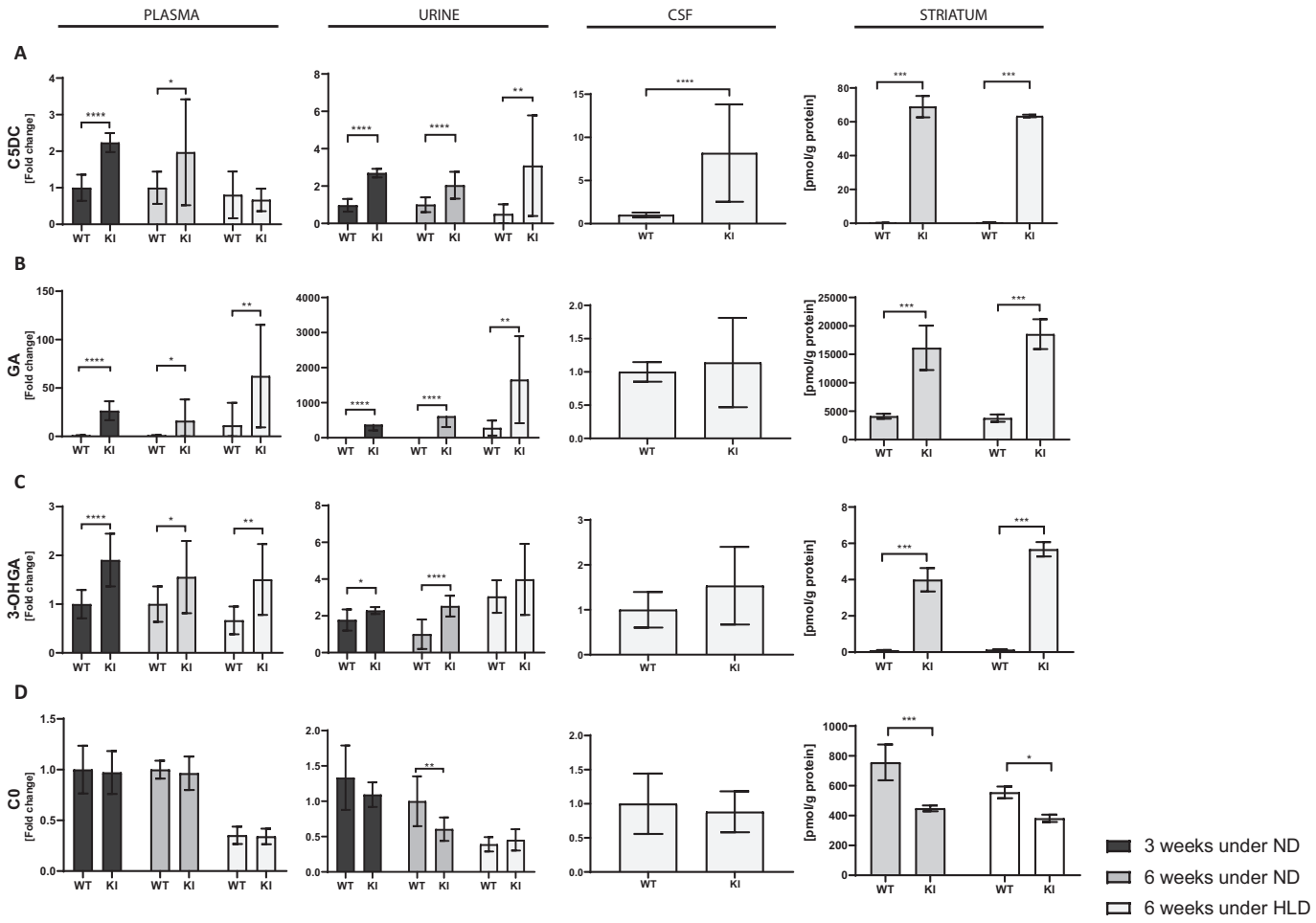

Fig. 2. High excretor phenotype of *Gcdh*$^{ki/ki}$ (KI) rats. Acylcarnitines and organic acids were measured in plasma (**first column**) and urine (**second column**) of WT and *Gcdh*$^{ki/ki}$ (KI) rats at 3 weeks (after weaning) under ND and at 6 weeks under ND and under HLD. CSF (**third column**) was only analyzed in 6-week-old rats under HLD. Striatal tissue (**fourth column**) was analyzed in 6-week-old WT and *Gcdh*$^{ki/ki}$ (KI) rats under ND and HLD. (**A**) Glutarylcarnitine (C5DC). (**B**) Glutaric acid (GA). (**C**) 3-Hydroxyglutaric acid (3OHGA). (**D**) Free Carnitine (C0). X-axes show genotypes, y-axes indicate fold changes. n = 4 for each condition. Data shown as mean ± SD; Student's *t*-test: $^{*}p < 0.05$, $^{**}p < 0.01$, $^{***}p < 0.001$, $^{****}p < 0.0001$.

and 0.0001) and a significantly reduced BMI ($P = 0.008$; Fig. 3G and H). After 21 days of HLD, *Gcdh*$^{ki/ki}$ rats appeared to be significantly smaller than WT rats under the same condition (Fig. 3H).

3.4. Neurological phenotype in *Gcdh*$^{ki/ki}$ rats under HLD

After one week of HLD, 4-week-old *Gcdh*$^{ki/ki}$ rats presented with lethargy, imbalance, muscle stiffness and spasticity (Supplementary Video 1) compared to *Gcdh*$^{ki/ki}$ rats under ND (Supplementary Video 2).

3.5. Ammonium increase and alterations of related metabolites in *Gcdh*$^{ki/ki}$ rats

Ammonium (NH_4^+; Fig. 4A): Under ND, plasma NH_4^+ concentrations increased significantly in *Gcdh*$^{ki/ki}$ rats compared to WT rats ($P < 0.001$). HLD induced a significant increase of NH_4^+ concentrations in *Gcdh*$^{ki/ki}$ and WT rats as compared to ND ($P < 0.001$), but NH_4^+ concentrations were still significantly higher in *Gcdh*$^{ki/ki}$ rats ($P = 0.013$).

Urea (Fig. 4B): Under HLD, urea was strongly decreased in plasma of *Gcdh*$^{ki/ki}$ rats ($P = 0.001$).

Glutamate (Glu; Fig. 4C-D): HLD induced a significant increase of Glu concentrations in plasma of WT rats under HLD (Fig. 4C), but not in *Gcdh*$^{ki/ki}$ rats. No significant changes were observed in urine (Fig. 4D).

Glutamine (Gln; Fig. 4E-F): A tendency for a decrease of Gln concentrations was noticed in plasma of *Gcdh*$^{ki/ki}$ rats under ND and HLD (Fig. 4E). In urine, an increase of Gln concentrations was observed in *Gcdh*$^{ki/ki}$ rats after exposure to HLD ($P < 0.0001$; Fig. 4F).

Ornithine (Orn; Fig. 4G-H): Under HLD, plasmatic Orn concentrations decreased significantly in WT and *Gcdh*$^{ki/ki}$ rats as compared to ND, but the decrease was more important in *Gcdh*$^{ki/ki}$ rats ($P = 0.02$; Fig. 4G). In contrast, urinary Orn concentrations increased significantly in *Gcdh*$^{ki/ki}$ rats under HLD ($P = 0.01$; Fig. 4H).

Arginine (Arg; Fig. 4I-J): Under HLD, plasmatic Arg concentrations increased to a similar extent in WT and *Gcdh*$^{ki/ki}$ rats ($P = 0.001$; Fig. 4I). In urine, a significant increase of Arg concentrations was observed in *Gcdh*$^{ki/ki}$ rats under ND and HLD ($P = 0.02$ and $P = 0.0001$ respectively; Fig. 4J).

3.6. Normal CPS1 activity in liver of *Gcdh* $^{ki/ki}$ rats

No significant difference in CPS1 enzymatic activities measured in liver tissue was observed between 6-week-old *Gcdh* $^{ki/ki}$ and WT rats under ND and HLD (data not shown).

3.7. Altered lysine degradation in *Gcdh*$^{ki/ki}$ rats under HLD

In order to search for potential changes in lysine degradation pathways, we measured lysine, aminoadipic acid, pipecolic acid and saccharopine concentrations in plasma, urine, CSF and striatum of 6-week-old *Gcdh*$^{ki/ki}$ and WT rats under ND and HLD (Fig. 5A-D).

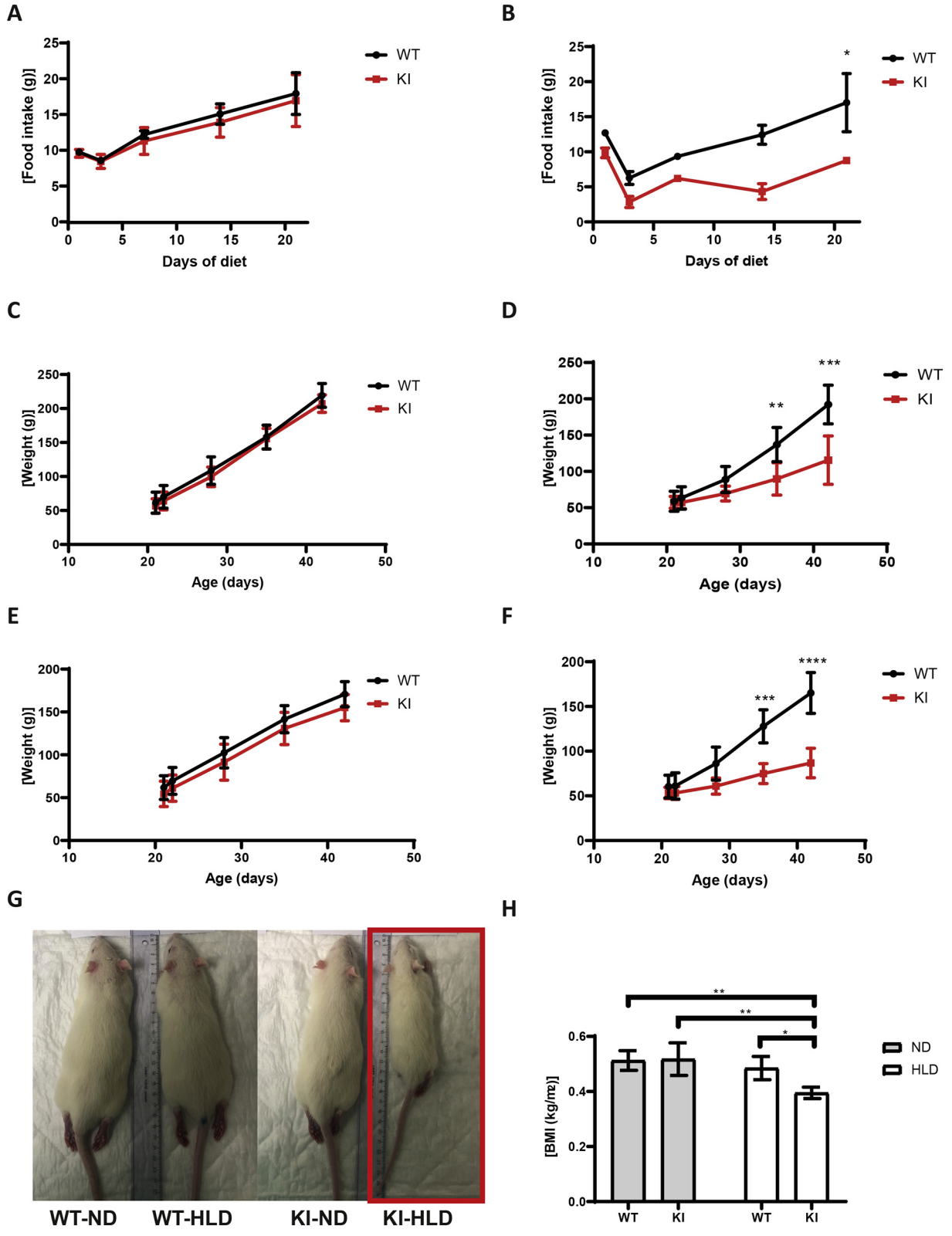

Fig. 3. Significantly decreased food intake led to reduced weight gain, lower BMI and smaller size in *Gcdh*$^{ki/ki}$ (KI) rats under HLD. WT and *Gcdh*$^{ki/ki}$ (KI) rats at the age of 3 weeks were fed during 21 days with either ND or HLD. Food intake was measured daily and rats were weighed once a week during the experiment. **A-F:** Results of WT rats are indicated in **black**, results of *Gcdh*$^{ki/ki}$ (KI) rats in **red**. (**A**) ND: Food intake of WT and *Gcdh*$^{ki/ki}$ (KI) rats under ND did not show any difference. (**B**) HLD: Under HLD, *Gcdh*$^{ki/ki}$ (KI) rats had a significantly lower food intake as compared to WT rats. (**C**) Males under ND: Weight gain did not differ between WT and *Gcdh*$^{ki/ki}$ (KI) males under ND. (**D**) Males under HLD: Under HLD, *Gcdh*$^{ki/ki}$ (KI) males had a significantly lower weight gain as compared to WT males. (**E**) Females under ND: Under ND, *Gcdh*$^{ki/ki}$ (KI) females had a slightly, but not significantly lower weight gain. (**F**) Females under HLD: Under HLD, *Gcdh*$^{ki/ki}$ (KI) females had a significantly lower weight gain. Data shown as mean ± SD; Student's test: $^{*}p < 0.05$, $^{**}p < 0.01$, $^{***}p < 0.001$, $p < 0.0001$. (**G**) Photos of WT and *Gcdh*$^{ki/ki}$ (KI) rats at the age of 6 weeks under ND and after 21 days of HLD. *Gcdh*$^{ki/ki}$ (KI) rats under HLD showed a significantly smaller body size (in red box). (**H**) Calculated BMI at the age of 6 weeks. Under HLD, *Gcdh*$^{ki/ki}$ (KI) rats had a significantly lower BMI than WT rats. Data shown as mean ± SD; Tukey test or Mann Whitney: $^{*}p < 0.05$, $^{**}p < 0.01$. (For interpretation of the references to colour in this figure legend, the reader is referred to the web version of this article.)

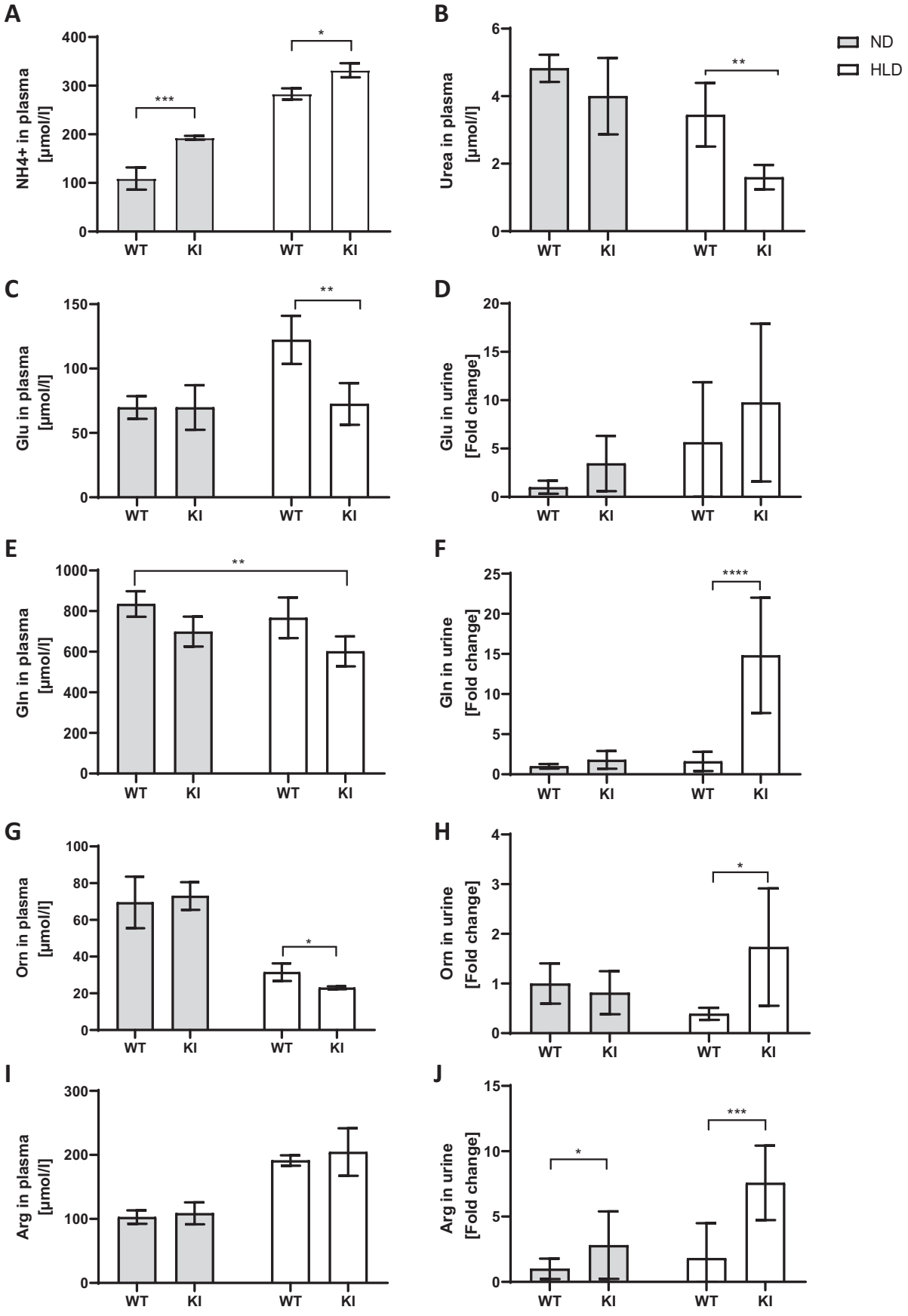
A
NH4+ in plasma [µmol/l]
400
300
200
100
0
***
*
WT
KI
WT
KI
B
Urea in plasma [µmol/l]
6
4
2
0
**
WT
KI
WT
KI
ND
HLD
C
Glu in plasma [µmol/l]
150
100
50
0
**
WT
KI
WT
KI
D
Glu in urine [Fold change]
20
15
10
5
0
WT
KI
WT
KI
E
Gln in plasma [µmol/l]
1000
800
600
400
200
0
**
WT
KI
WT
KI
F
Gln in urine [Fold change]
25
20
15
10
5
0
****
WT
KI
WT
KI
G
Orn in plasma [µmol/l]
100
80
60
40
20
0
*
WT
KI
WT
KI
H
Orn in urine [Fold change]
4
3
2
1
0
*
WT
KI
WT
KI
I
Arg in plasma [µmol/l]
300
200
100
0
WT
KI
WT
KI
J
Arg in urine [Fold change]
15
10
5
0
*
***
WT
KI
WT
KI

Kynurenine was only analyzed in plasma (Fig. 5E). Measurements of lysine, aminoadipic acid and pipecolic acid concentrations in CSF under HLD did not reveal any significant differences between WT and *Gcdh*$^{ki/ki}$ rats (data not shown).

Lysine (Lys; Fig. 5A): As expected, plasmatic Lys concentrations increased significantly in both genotypes under HLD compared to ND ($P = 0.000$). In urine, Lys concentrations increased significantly in *Gcdh*$^{ki/ki}$ rats exposed to HLD ($P = 0.0001$). Lys increased significantly in striatum of *Gcdh*$^{ki/ki}$ rats under ND and HLD ($P = 0.000$).

Aminoadipic acid (Fig. 5B): Aminoadipic acid increased after exposure to HLD in both, WT and *Gcdh*$^{ki/ki}$ rats in plasma, urine and striatum ($P = 0.000$ for each one). No difference was observed between WT and *Gcdh*$^{ki/ki}$ rats under ND or HLD.

Pipecolic acid (Fig. 5C): Only low concentrations of pipecolic acid were detected in plasma and urine of WT and *Gcdh*$^{ki/ki}$ rats under ND. Surprisingly, concentrations of pipecolic acid increased significantly in plasma, urine and striatum of *Gcdh*$^{ki/ki}$ rats under HLD ($P = 0.000$, $P < 0.0001$ and $P < 0.000$). Pipecolic acid was found to be already significantly increased after 24 h of HLD in plasma of *Gcdh*$^{ki/ki}$ rats (data not shown).

Saccharopine (Fig. 5D): Saccharopine concentrations were only analyzed in plasma and urine. Under HLD, saccharopine concentrations showed a significant decrease in plasma ($P = 0.01$) and a significant increase in urine ($P = 0.0001$) of *Gcdh*$^{ki/ki}$ rats.

Kynurenine (Fig. 5E): Kynurenine concentrations were only analyzed in plasma. A significant decrease of kynurenine was observed in plasma of *Gcdh*$^{ki/ki}$ rats under HLD ($P = 0.000$).

3.8. Amino acid alterations in *Gcdh*$^{ki/ki}$ rats

A panel of amino acids was investigated by LC-MS/MS or UHPLC in plasma, urine, CSF and striatum of 6-week-old *Gcdh*$^{ki/ki}$ and WT rats under ND and HLD. Apart from the above-mentioned amino acids, nine other amino acids presented significant differences between *Gcdh*$^{ki/ki}$ and WT rats in at least two body samples:

Glycine (Supp. Fig. 1a A): Under HLD, glycine was found to be significantly lower in plasma of WT and *Gcdh*$^{ki/ki}$ rats ($P = 0.000$) compared to WT and *Gcdh*$^{ki/ki}$ rats under ND. Glycine was found significantly increased in urine ($P = 0.0001$) and decreased in CSF of *Gcdh*$^{ki/ki}$ rats under HLD ($P = 0.01$) compared to WT rats under HLD. No significant changes were observed in striatum.

Histidine (Supp. Fig. 1a B): Under HLD, histidine concentrations were found significantly increased in urine and CSF of *Gcdh*$^{ki/ki}$ rats ($P = 0.0001$ and $P = 0.0006$ respectively) compared to WT rats under HLD. No significant changes were observed in plasma and striatum.

Homocitrulline (Supp. Fig. 1a C): Homocitrulline concentrations were significantly increased in plasma, urine, CSF and striatum of *Gcdh*$^{ki/ki}$ rats under HLD ($P = 0.02$, $P = 0.0001$, $P = 0.0001$ and $P = 0.000$ respectively) compared with WT rats under HLD.

Methionine (Supp. Fig. 1a D): Methionine concentrations were significantly lower in plasma of *Gcdh*$^{ki/ki}$ rats under HLD ($P = 0.013$) compared with WT rats under HLD, while its urinary excretion and concentrations in CSF increased under the same condition ($P = 0.009$). No significant changes were observed in urine and striatum.

Leucine (Supp. Fig. 1a E): A significant decrease of leucine concentrations was observed in plasma of *Gcdh*$^{ki/ki}$ rats independently of diet as compared to WT rats, while leucine concentrations increased significantly in urine of *Gcdh*$^{ki/ki}$ rats under HLD ($P = 0.0083$). No significant changes were observed in CSF and striatum.

Phenylalanine (Supp. Fig. 1b F): Under ND, urinary phenylalanine excretion was significantly higher in *Gcdh*$^{ki/ki}$ rats ($P = 0.03$) compared to WT rats under ND. Under HLD, plasmatic phenylalanine concentrations revealed a significant decrease in both genotypes, but the decrease was more important in *Gcdh*$^{ki/ki}$ rats ($P = 0.04$) compared to WT rats under HLD. No significant changes were observed in CSF and striatum.

Serine (Supp. Fig. 1b G): Independently of the diet, serine tended to increase in *Gcdh*$^{ki/ki}$ rats in all performed analyses. It was significantly increased in urine and striatum of *Gcdh*$^{ki/ki}$ rats under both diets compared to WT rats (urine ND: $P = 0.03$, urine HLD: $P = 0.04$, striatum ND: $P = 0.004$ and striatum HLD: $P = 0.001$) and in plasma of *Gcdh*$^{ki/ki}$ rats under HLD ($P = 0.046$).

Valine (Supp. Fig. 1b H): Under HLD, valine concentrations decreased significantly in plasma of *Gcdh*$^{ki/ki}$ rats compared to WT rats under HLD ($P = 0.003$). In striatum, valine concentrations increased in *Gcdh*$^{ki/ki}$ rats under ND and HLD compared to WT rats. No significant changes were observed in urine and CSF.

Taurine (Supp. Fig. 1b I): Taurine concentrations increased significantly in plasma and urine of *Gcdh*$^{ki/ki}$ rats under HLD ($P = 0.02$ and $P = 0.0067$) compared to WT rats under HLD. No significant changes were observed in CSF and striatum.

The results for the following amino acids did not reveal any significant differences: alanine, asparagine, aspartate, citrulline, cystine, ethanolamine, hydroxylysine, hydroxyproline, oxidised glutathione, phosphoethanolamine, proline, sarcosine, anthranilic acid, xanthurenic acid, tryptophane, tyrosine and creatinine (data not shown).

3.9. Altered brain metabolism in *Gcdh*$^{ki/ki}$ rats

We evaluated brain metabolism in WT and *Gcdh*$^{ki/ki}$ rats at the age of 6 weeks under ND and HLD by analyses of amino acids and organic acids in CSF and brain tissue (striatum) and by 1H-MRS of the rat striatum using a high magnetic field of 9.4 T (Fig. 6). Data for CSF metabolites were only available in 6-week-old rats under HLD.

Glutamate (Glu; Fig. 6A-C): Under HLD, 1H-MRS of the striatum showed a decrease of 10% Glu in *Gcdh*$^{ki/ki}$ rats ($P = 0.007$). No significant difference was observed in CSF and striatal tissue.

Glutamine (Gln; Fig. 6D-F): 1H-MRS revealed a decrease of 15% Gln in striatum of *Gcdh*$^{ki/ki}$ rats under ND ($P = 0.008$) and an increase in both genotypes under HLD (52% in WT rats and 80% in *Gcdh*$^{ki/ki}$ rats). Under HLD, Gln increased significantly in CSF of *Gcdh*$^{ki/ki}$ rats ($P = 0.0002$). A trend to decrease was observed in striatal tissue, but it was not statistically significant.

Creatine (Fig. 6G-I): Under HLD, creatine concentrations decreased significantly in CSF of *Gcdh*$^{ki/ki}$ rats ($P = 0.01$). In striatal tissue, creatine decreased significantly in WT rats under HLD ($P = 0.012$), while no significant difference was observed by 1H-MRS.

Lactate (Fig. 6J-K): Under HLD, lactate significantly decreased in CSF of *Gcdh*$^{ki/ki}$ rats ($P = 0.006$). 1H-MRS in striatum revealed a lactate increase in both genotypes under HLD (48% in WT rats and 44% in *Gcdh*$^{ki/ki}$ rats, $P = 0.001$). However, 1H-MRS did not reveal any significant difference between WT and *Gcdh*$^{ki/ki}$ rats under ND or HLD. Lactate was also measured in plasma and urine, but no significant changes were observed (data not shown). It was not analyzed in striatal tissue.

Fig. 4. Increased ammonium and decreased urea concentrations in plasma of *Gcdh*$^{ki/ki}$ (KI) rats under HLD. Different metabolites were measured in 6-week-old WT and *Gcdh*$^{ki/ki}$ (KI) rats under ND or after 21 days of HLD in plasma (quantitative analyses) and urine (semi-quantitative analyses by UHPLC). (**A**) Ammonium ($NH4^+$) concentrations in plasma showed a significant increase in *Gcdh*$^{ki/ki}$ (KI) rats under ND and HLD. (**B**) Urea concentrations in plasma revealed a significant decrease in *Gcdh*$^{ki/ki}$ (KI) rats under HLD. (**C**) Glutamate (Glu) concentrations in plasma showed a significant decrease in *Gcdh*$^{ki/ki}$ (KI) rats under HLD. (**D**) Glu concentrations in urine. (**E**) Glutamine (Gln) concentrations in plasma. (**F**) Gln concentrations in urine revealed a significant increase in *Gcdh*$^{ki/ki}$ (KI) rats under HLD. (**G**) Ornitine (Orn) concentrations in plasma showed a significant decrease in *Gcdh*$^{ki/ki}$ (KI) rats under HLD, while Orn concentrations in urine (**H**) increased significantly in the same condition. (**I**) Arginine (Arg) concentrations in plasma. (**J**) Arg concentrations in urine revealed a significant increase in *Gcdh*$^{ki/ki}$ (KI) rats under ND and even more pronounced under HLD. $n = 4$ for all conditions. X-axes show genotypes. Data shown as mean ± SD; multiple comparisons Tukey test or Mann Whitney: *$p < 0.05$, **$p < 0.01$, ***$p < 0.001$ after ANOVA two ways analysis. Data shown as mean ± SD: Student's t-test: ****$p < 0.0001$.

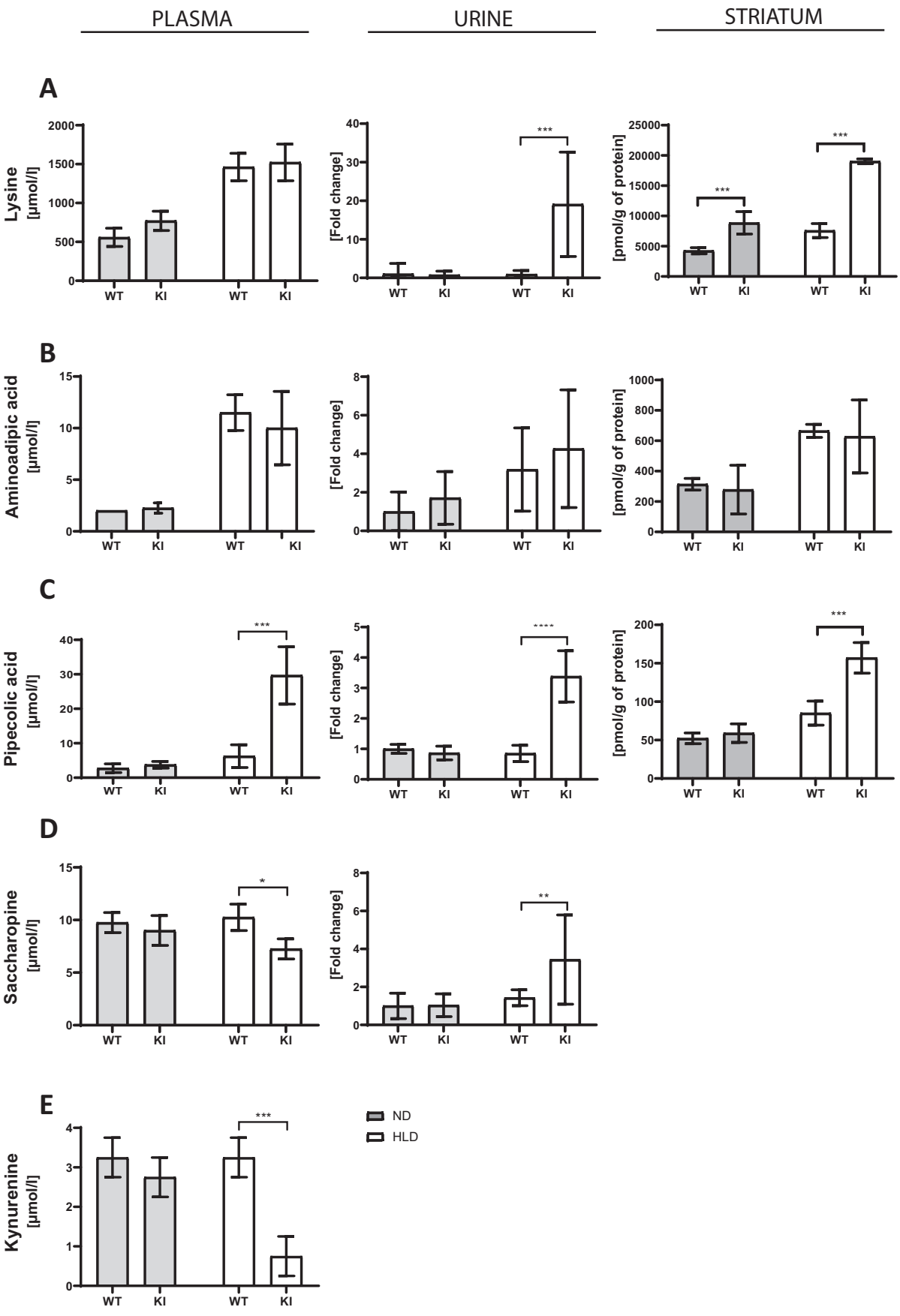
PLASMA
URINE
STRIATUM
A
Lysine [µmol/l]
[Fold change]
[pmol/g of protein]
B
Aminoadipic acid [µmol/l]
C
Pipecolic acid [µmol/l]
D
Saccharopine [µmol/l]
E
Kynurenine [µmol/l]
WT
KI
ND
HLD

Myo-inositol (Fig. 6L): Under HLD, 1H-MRS revealed a significant decrease (18%) of myo-inositol in striatum of *Gcdh*$^{ki/ki}$ rats ($P = 0.013$). It was not analyzed in striatal tissue or CSF.

Inosine (Fig. 6M): Under HLD, inosine decreased significantly in CSF of *Gcdh*$^{ki/ki}$ rats ($P = 0.006$). It was not analyzed in striatum, neither in tissue nor by 1H-MRS.

Gamma-aminobutyric acid (GABA): No significant changes were observed for GABA in CSF, striatal tissue or by 1H-MRS (data not shown).

3.10. Increased vacuole numbers in different brain regions of *Gcdh*$^{ki/ki}$ rats

Brains of 6-week-old rats under ND and HLD were cut in sagittal sections, stained with HE and analyzed in a standardized manner (Fig. 7). We detected an increased number of optically empty vacuoles in *Gcdh*$^{ki/ki}$ brains compared to WT brains. Spongiotic changes were most pronounced in the corpus callosum until the fornix (Fig. 7E) and in the striatum of *Gcdh*$^{ki/ki}$ rats under HLD (Fig. 7I). In the anterior commissural nucleus (Fig. 7K and M) and the cerebellum (Fig. 7O and Q), the number of vacuoles increased in *Gcdh*$^{ki/ki}$ rats independently of the type of diet In general, these vacuoles appeared as irregularly distributed spongiotic changes within white matter. Electron microscopy revealed no cellular reaction like gliosis or necrosis (data not shown). Quantification of vacuoles in corpus callosum (Fig. 7R) and striatum (Fig. 7S) showed a significant increase in 4/4 *Gcdh*$^{ki/ki}$ rats exposed to HLD. In the anterior commissural nucleus (Fig. 7T) and the cerebellum (Fig. 7U) vacuole numbers were increased in 4/4 *Gcdh*$^{ki/ki}$ rats under ND and in 4/4 *Gcdh*$^{ki/ki}$ rats under HLD independently of gender (2 males and 2 females). Luxol fast blue-stained sections did not show any myelin loss and PAS staining did not reveal any significant differences in proportion of macromolecules like glycogen and proteoglycans (data not shown).

3.11. Co-localization of microglial activation and astrogliosis in *Gcdh*$^{ki/ki}$ rat brains

Immunostaining for Iba-1 in WT rats under ND revealed small cellular bodies and well-developed dendritic prolongations (Fig. 8A-B). In 6-week-old *Gcdh*$^{ki/ki}$ rats, Iba-1-immunoreactive microglia showed hypertrophic cytoplasm and retracted processes independently of the diet in striatum, cerebellum, hippocampus and cortex (for cerebellum see Fig. 8; for hippocampus see Fig. 9; data not shown for striatum and cortex). However, staining for Iba-1 in cerebellum of *Gcdh*$^{ki/ki}$ rats under HLD revealed an amoeboid morphology of microglia (Fig. 8G-H) compared to WT rats under HLD (Fig. 8E-F). This observation was also present, but less pronounced in cerebellum of *Gcdh*$^{ki/ki}$ rats under ND (Fig. 8C-D). Co-staining for Iba1 and GFAP confirmed microglial activation in hippocampus of *Gcdh*$^{ki/ki}$ rats under ND and HLD (Fig. 9B and D).

Immunostaining for GFAP in different brain regions of 6-week-old *Gcdh*$^{ki/ki}$ rats under ND and HLD showed the typical signs for astrogliosis: an increased diameter of cell bodies and increased thickness of proximal processes of astrocytes, which often were found aggregated together (Fig. 9). Co-immunostaining for GFAP and Iba1 showed astrogliosis in *Gcdh*$^{ki/ki}$ rats independently of the diet in hippocampus (Fig. 9A-D), striatum, cerebellum and cortex (data not shown). These are the same regions, in which microglial activation was observed (see above).

3.12. Apoptotic cell death of cerebellar astrocytes in *Gcdh*$^{ki/ki}$ rats under ND

Immunostaining for DAPI and cleaved caspase 3 showed an increased cell death by apoptosis in the granular layer and white matter of the cerebellum in *Gcdh*$^{ki/ki}$ rats under ND (Fig. 10A-B). Co-staining with GFAP identified astrocytes as the dying cells (Fig. 10C-D). No increased cell death or apoptosis was observed in other brain regions of *Gcdh*$^{ki/ki}$ rats under ND or HLD (data not shown).

3.13. Combined effect of genotype and diet on cerebellar neurons in *Gcdh*$^{ki/ki}$ rats under HLD

Immunostaining for MAP2 showed a decreased signal in cerebellum of 6-week-old *Gcdh*$^{ki/ki}$ rats under ND (Fig. 10F). The effects of genotype and diet were additive and resulted in the most severe decrease of MAP2 expression in cerebellar neurons of *Gcdh*$^{ki/ki}$ rats under HLD (Fig. 10H). No significant difference was observed between *Gcdh*$^{ki/ki}$ and WT rats under HLD in other brain regions or under ND (data not shown). However, proteomic analyses showed downregulation of MAP2 in striatum of *Gcdh*$^{ki/ki}$ rats under HLD (Suppl. Table 5).

3.14. Altered OXPHOS activities in hippocampus and striatum of *Gcdh*$^{ki/ki}$ rats

Enzymatic activities and western blot analyses of the five OXPHOS complexes were analyzed in cortex, cerebellum, hippocampus and striatum of 6-week-old WT and *Gcdh*$^{ki/ki}$ rats under ND and HLD. No significant differences between WT and *Gcdh*$^{ki/ki}$ rats were found for enzymatic OXPHOS activities in cerebellum and cortex (data not shown).

In hippocampus, activity of complex IV (cytochrome *c* oxidase) increased significantly in *Gcdh*$^{ki/ki}$ rats under ND (Fig. 11D). We also observed a slightly increased, but statistically not significant activity of complex IV (cytochrome *c* oxidase) in hippocampus of *Gcdh*$^{ki/ki}$ rats under HLD (Fig. 11D).

In striatum, enzymatic activity of complex I (NADH:ubiquinone oxidoreductase) was found significantly increased in *Gcdh*$^{ki/ki}$ rats under ND (Fig. 11F), while activities of complexes III (cytochrome *c* reductase) and IV decreased significantly (Fig. 11H-I) in the same condition. No significant difference was observed in rats under HLD.

Western blot analyses of the five OXPHOS complexes did not show any significant differences between WT and *Gcdh*$^{ki/ki}$ rats under ND and HLD (data not shown).

3.15. Altered whole brain proteome of *Gcdh*$^{ki/ki}$ rats

Protein expression profiles have been investigated in whole brain tissues of 3- and 6-week-old WT and *Gcdh*$^{ki/ki}$ rats under ND by a quantitative label-free proteomic approach comparing the brain protein abundance between *Gcdh*$^{ki/ki}$ and WT rats (Fig. 12).

In whole brain analyses of 3-week-old rats, 346 proteins were found statistically altered in *Gcdh*$^{ki/ki}$ rats compared to WT rats; among these, 198 proteins were down-regulated and 148 were up-regulated (Fig. 12A-B, Supp. Table 1). Significant protein alterations were graphically represented in a volcano plot (Fig. 12A), highlighting the significant down- (blue) and up-regulated (red) proteins and in a heat map overview (Fig. 12B) showing a good separation between *Gcdh*$^{ki/ki}$ and WT rats.

Fig. 5. Lysine degradation via pipecolic acid pathway in *Gcdh*$^{ki/ki}$ (KI) rats under HLD. The following metabolites implicated in Lys degradation were analyzed in 6-week-old WT and *Gcdh*$^{ki/ki}$ (KI) rats under ND or after 21 days of HLD in plasma (quantitative analyses, **first column**), urine (semi-quantitative analyses by UHPLC, **second column**) and in striatal tissue (quantitative analyses, third **column**): (**A**) Lysine, (**B**) aminoadipic acid, (**C**) pipecolic acid and (**D**) saccharopine. Under HLD, pipecolic acid increased significantly in plasma, urine and striatum of *Gcdh*$^{ki/ki}$ (KI) rats. n = 4 for each conditions. X-axes show genotypes. Data shown as mean ± SD; Tukey test (plasma and striatum) and Student's t-test or Mann Whitney (urine and CSF): *p < 0.05, **p < 0.01, ***p < 0.001, ****p < 0.0001.

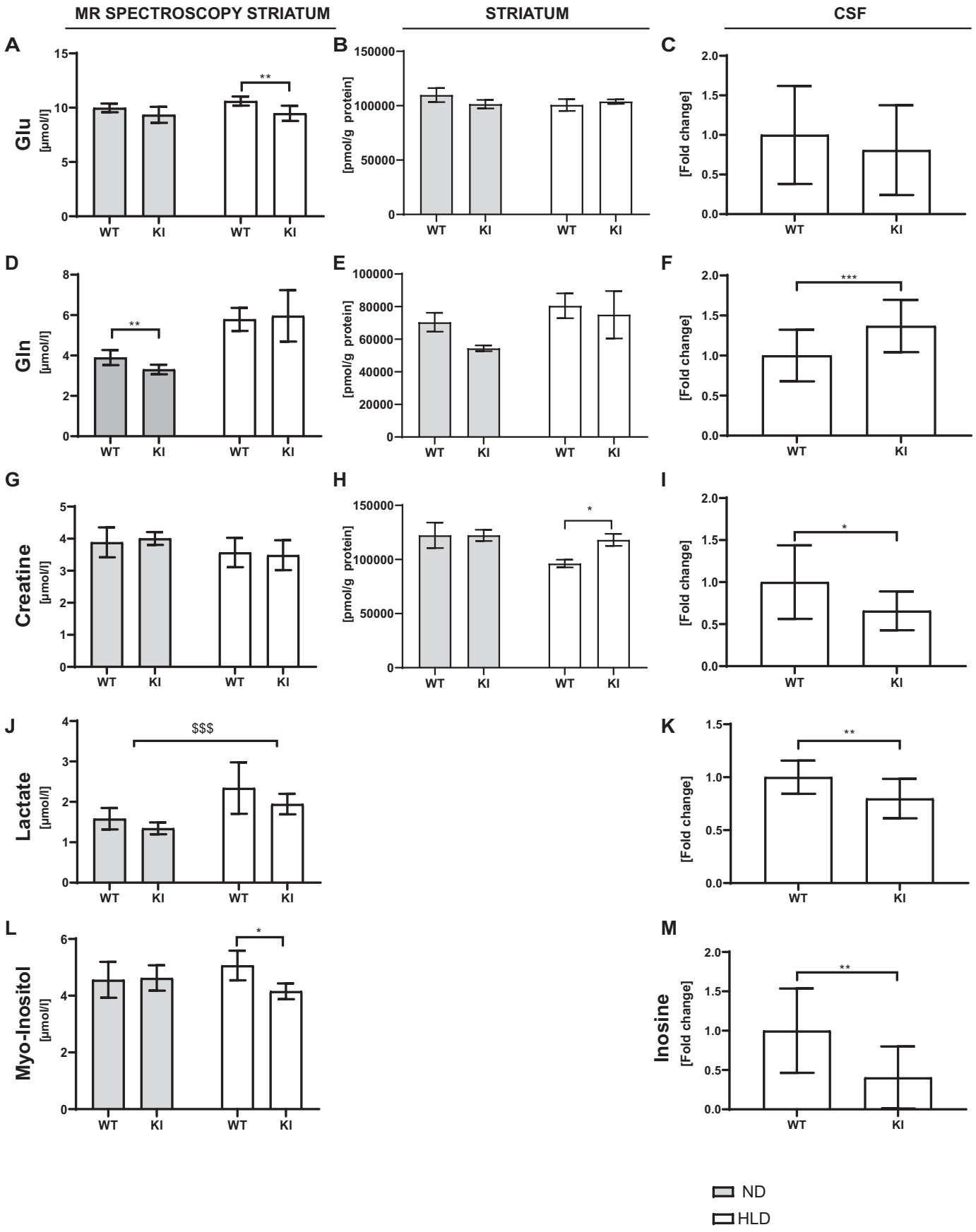
MR SPECTROSCOPY STRIATUM
STRIATUM
CSF
A
Glu
[µmol/l]
B
[pmol/g protein]
C
[Fold change]
D
Gln
[µmol/l]
E
[pmol/g protein]
F
[Fold change]
G
Creatine
[µmol/l]
H
[pmol/g protein]
I
[Fold change]
J
Lactate
[µmol/l]
K
[Fold change]
L
Myo-Inositol
[µmol/l]
M
Inosine
[Fold change]
WT
KI
**
*
***
$$$
ND
HLD

In whole brain analyses of 6-week-old rats, comparative analysis resulted in the identification of 392 differentially regulated proteins in *Gcdh*$^{ki/ki}$ rats, of which 318 proteins resulted up-represented and 74 down-represented (Fig. 12C-D, for a detailed list see Supp. Table 2).

A total of 41 up-regulated and 15 down-regulated proteins were identified in common at the age of 3 and 6 weeks (Fig. 12E-F, for a detailed list see Supp. Table 3).

The lists of significant differentially expressed proteins in *Gcdh*$^{ki/ki}$ rats compared to WT rats, of which the relative abundance was also influenced by age and diet, were clustered according to their gene ontology (GO) categories. The most interesting altered GO molecular function in *whole brains of Gcdh*$^{ki/ki}$ *rats at the age of 3 weeks under ND* was 'structural postsynaptic constituents` (*p*-value 6.54E-06, n. intersections 6) (Fig. 12G and Supp. Table 4). According to GO biological process clusterization, the processes 'nervous system development' (*p*-value 3.02E-11, n. intersections 71), 'synaptic signaling' (*p*-value 2.70E-10, n. intersections 34), and 'neuron projection development' (*p*-value 2.12E-8, n. intersections 39) were the most affected (Fig. 12G and Supp. Table 4). For GO cellular component analysis, 78 dysregulated proteins were recognized as belonging to the 'synapse' (*p*-value 1.55E-35) (Fig. 12G and Supp. Table 4).

In whole brains of 6-week-old Gcdh$^{ki/ki}$ *rats under ND*, the GO biological processes 'nervous system development' (*p*-value 2.02E-07, n. intersections 65), 'synaptic signaling' (*p*-value 6.65E-08, n. intersections 32), and 'neuron projection development' (*p*-value 9.51E-07, n. intersections 38) were found commonly enriched (Fig. 12H and Supp. Table 5). As for 3-week-old rats, the most significant GO cell component enriched in 6-week-old *Gcdh*$^{ki/ki}$ whole brains under ND was 'synapse' with 84 dysregulated proteins (*p*-value 6.15E-37). Differentially abundant proteins were also analyzed using the REACTOME, KEGG, and human phenotype (HP) databases (Fig. 12G, H and Supp. Tables 4–5). In particular, the KEGG clustering showed 'biosynthesis of amino acids' (*p*-value 7.16E-10, n. intersections 15) and 'carbon metabolism' (*p*-value 4.01E-09, n. intersections 17) as major significant clusters. Interestingly, the HP class 'abnormal muscle physiology' (*p*-value 4.12E-3, n. intersections 53) was also found enriched in the differential proteome of 6-week-old rats under ND.

The common differential abundant proteins between *Gcdh*$^{ki/ki}$ whole brains at 3 and 6 weeks under ND (Supp. Table 3) were also clustered according to GO and the most significant cluster was associated with 'chaperone complex' (*p*-value 2.09E-5, n. intersections 4) (Supp. Table 6).

3.16. Altered striatum proteome of *Gcdh*$^{ki/ki}$ rats

In order to investigate the interaction between genotype and nutritional Lys intake, differential protein expressions were measured *in striatum of 6-week-old rats under ND and HLD* (Fig. 13). In striatum of *Gcdh*$^{ki/ki}$ rats under ND, a total of 197 protein alterations were identified, of which 144 proteins resulted down-represented and 53 up-represented in comparison to WT rats (Fig. 13A-B, for a detailed list see Supp. Table 7). Under HLD, *Gcdh*$^{ki/ki}$ rats showed an altered expression of 116 proteins, among which 84 were less abundant and 32 more abundant in *Gcdh*$^{ki/ki}$ rats compared to WT rats (Fig. 13C-D, for a detailed list see Supp. Table 8). Comparing the striatal proteome of *Gcdh*$^{ki/ki}$ rats under ND and under HLD, 43 proteins were found downregulated (Fig. 13E) and 13 proteins up-regulated (Fig. 13F) in both conditions (Supp. Table 9). In addition, the relative abundance of 60 proteins (41 down-regulated and 19 up-regulated proteins) was found specifically affected by HLD in the striatum of *Gcdh*$^{ki/ki}$ rats, showing a cooperative behavior between genotype and environmental status (Supp. Table 10).

Analyses of *striatum of 6-week-old Gcdh*$^{ki/ki}$ *rats under ND* revealed enrichment of 19 proteins involved in the GO cell component 'glutamatergic synapse' (*p*-value 1.09E-10) (Fig. 13G and Supp. Tables 11). Analyses of *differential proteins in striatum of 6-week-old Gcdh*$^{ki/ki}$ versus *WT rats* showed 'nervous development' (*p*-value 2.83E-8, n. intersections 30) as the most significantly enriched GO biological process *in Gcdh*$^{ki/ki}$ *rats under ND* (Fig. 13G and Supp. Tables 11), and 'nervous system development' (*p*-value 1.32E-4, n. intersections 27) *in Gcdh*$^{ki/ki}$ *rats under HLD* (Fig. 13H and Supp. Tables 12).

The cluster enrichment analysis from the 56 *common abundant proteins in striatum of 6-week-old Gcdh*$^{ki/ki}$ *rats under ND or HLD* (Supp. Table 13) reveled 'synapse' (*p*-value 2.97E-4, n. intersections 12) and 'cell junction' (*p*-value 4.37E-4, n. intersections 13) as the most significant clusters (Supp. Table 13).

4. Discussion

4.1. Creation of the first rat model for GA-I

In this study, we present the first rat model for GA-I, carrying the rat sequence homologue (p.R411W) of the frequent Caucasian *GCDH* mutation p.R402W leading to a high excretor phenotype [48], which was also observed in *Gcdh*$^{ki/ki}$ rats. Western blotting showed a significantly diminished expression in kidney, liver and brain of *Gcdh*$^{ki/ki}$ rats compared with WT controls, suggesting that the *Gcdh* mutation p.R411W causes instability and early degradation. GCDH enzymatic activity assays showed a significant decrease of activity in heart, liver and kidney while no significant change was observed in brain. The lack of significant changes in brain may be explained by the low enzymatic activity detectable in this tissue. However, taking into consideration that neither *Gcdh*$^{-/-}$ mice nor *Gcdh*$^{ki/ki}$ rats present spontaneous AECs under ND, the potential existence of an alternative degradation pathway for glutaryl-CoA in rodent CNS would be an alternative explanation. The degradation of brain metabolites associated with glutaryl-CoA catabolic pathway are being further explored. Notably, our assay is following the production of 3-hydroxybutyryl-CoA and recent data indicates that its metabolism occurs at faster rates in brain tissue (data not shown). Due to the lack of a known specific enoyl-CoA hydratase inhibitor, our assay is limited by the fact that the direct product of GCDH reaction cannot be monitored.

4.2. Clinical observations during HLD

As *Gcdh*$^{-/-}$ mice, *Gcdh*$^{ki/ki}$ rats did not develop any spontaneous AEC. Stimulation of toxic metabolic production by HLD induced clinical signs of AEC like lethargy, imbalance, muscle stiffness and spasticity in *Gcdh*$^{ki/ki}$ rats. Further, a significant decrease of weight gain after 14 days explained by a concomitant decrease of daily food intake was observed in *Gcdh*$^{ki/ki}$ rats under HLD. In GA-I patients, periods of prolonged fasting before AEC were described. AECs were triggered by infections or catabolism of other origin and were associated with a pro-inflammatory state [49]. Our results are consistent with a recent multicenter study that reported the negative impact of non-adherence to emergency treatment on anthropometric long-term development in GA-I patients [50]. Loss of appetite (anorexia) is frequently associated with a

Fig. 6. Correlation between MR spectroscopy of the striatum, striatal tissue and CSF. 6-week-old WT and *Gcdh*$^{ki/ki}$ (KI) rats under ND or after 21 days of HLD underwent 1H-MRS of the striatum using a high magnetic field of 9.4 T (**left column**). Striatal tissue was obtained after decapitation and metabolites analyzed by LC-MS/MS (**middle column**). CSF was analyzed by semi-quantitative HPLC-LS/MS after HLD (**right column**). Significant alterations between WT and *Gcdh*$^{ki/ki}$ (KI) rats were obtained for the following metabolites: Glutamate (**A, B and C**), glutamine (**D, E and F**), creatine (**G, H and I**), lactate (**J and K**), myo-inositol (**L**) and inosine (**M**). $n = 5$ for each condition. X-axes show genotypes. Data shown as mean ± SD; Tukey test or Mann Whitney (striatum) after ANOVA two ways analysis or Kruskal Wallis and Mann Whitney (CSF): $^{*}p < 0.05$, $^{**}p < 0.01$, $^{***}p < 0.001$. $^{\$\$\$}p < 0.001$ differences between ND and HLD groups.

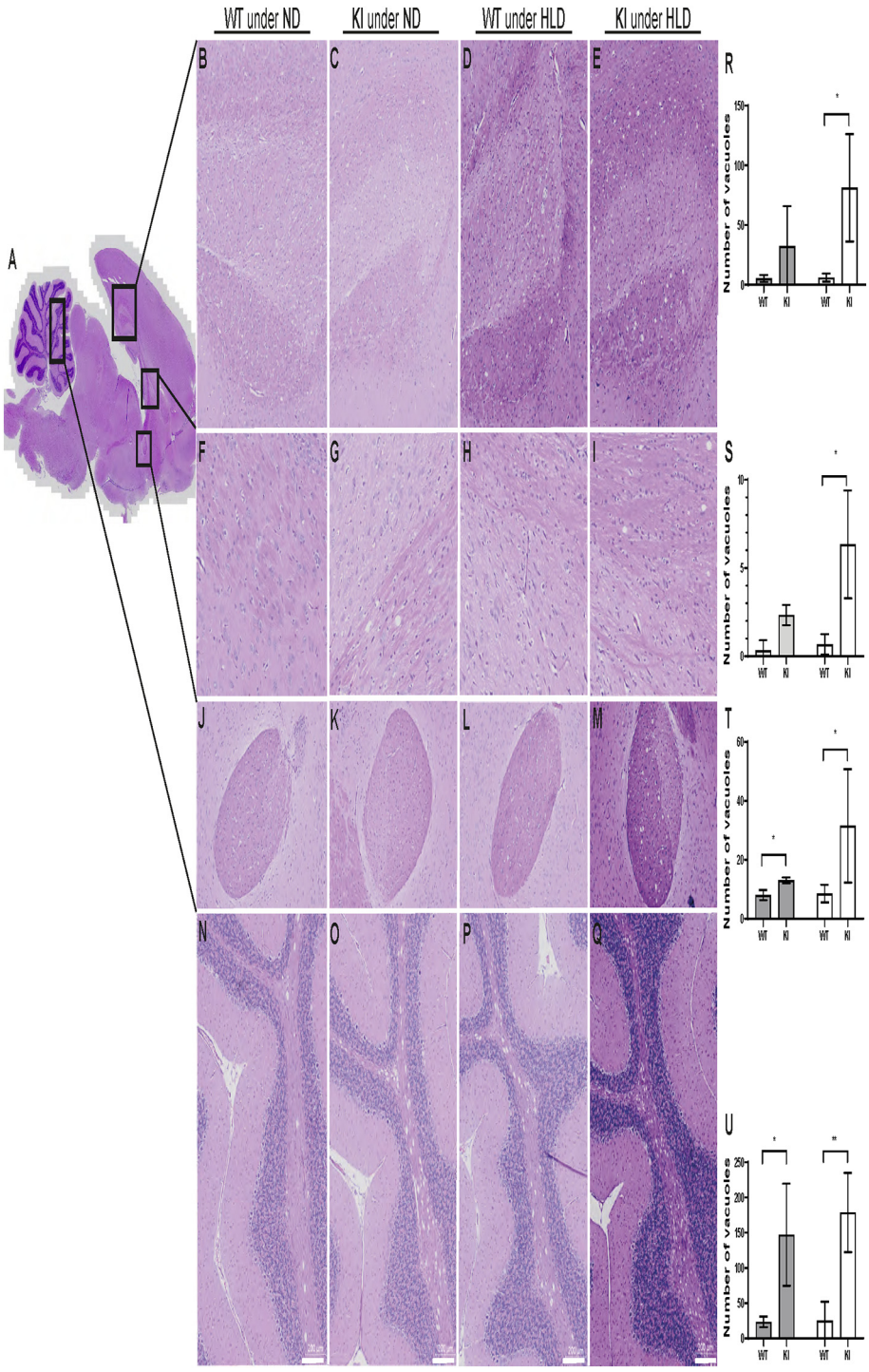

Fig. 7. HE stained brain sections of WT and *Gcdh*$^{ki/ki}$ (KI) rats under ND and HLD. (**A**) Localization of zoom images from corpus callosum (**B–E**), striatum (**F–I**) anterior commissural nucleus (**J–M**) and cerebellar white matter (**N–Q**) are shown with boxes on a sagittal section of rat brain at magnification 20×. Spongiotic changes were observed in *Gcdh*$^{ki/ki}$ (KI) rats under ND (**C, G, K and O**) and HLD (**E, I, M and Q**). WT controls under ND are shown in B, F, J and N and under HLD in D, H, L and P. Scale bar 200 μM. Quantification of vacuoles in corpus callosum (**R**), striatum (**S**), anterior commissural nucleus (**T**) and cerebellar white matter (**U**) of WT rats and *Gcdh*$^{ki/ki}$ (KI) rats under ND and under HLD. $n = 4$ for each condition. Data shown as mean ± SD; Tukey test or Mann Whitney $^{*}p < 0.05$, $^{**}p < 0.01$.

pro-inflammatory state. Almost all illnesses can impair appetite temporarily, but there are chronic diseases that can make loss of appetite worse. A weight loss of 15–40% indicates a poor prognosis. The role of interleukin induction in appetite loss has been well documented in cancer and infectious diseases and is required for optimal microglial activation [51,52]. Therefore, the decreased food intake observed in *Gcdh*$^{ki/ki}$ rats under HLD might be the consequence of a neuroinflammatory process shown by presence of microglial activation in our model.

Amino acids have been known for a long time to be the most efficient type of nutrient at satisfying hunger and providing an extended period of satiety. Moreover, different studies indicate that circulating concentrations of certain amino acids could influence food intake. Recent studies associated the Lys intake with satiety and appetite by control of ghrelin and leptin hormones in chickens [53]. In parallel, hypothalamic glial cells named tanycytes which are known to detect glucose in CSF, were identified to detect amino acids such as Lys and

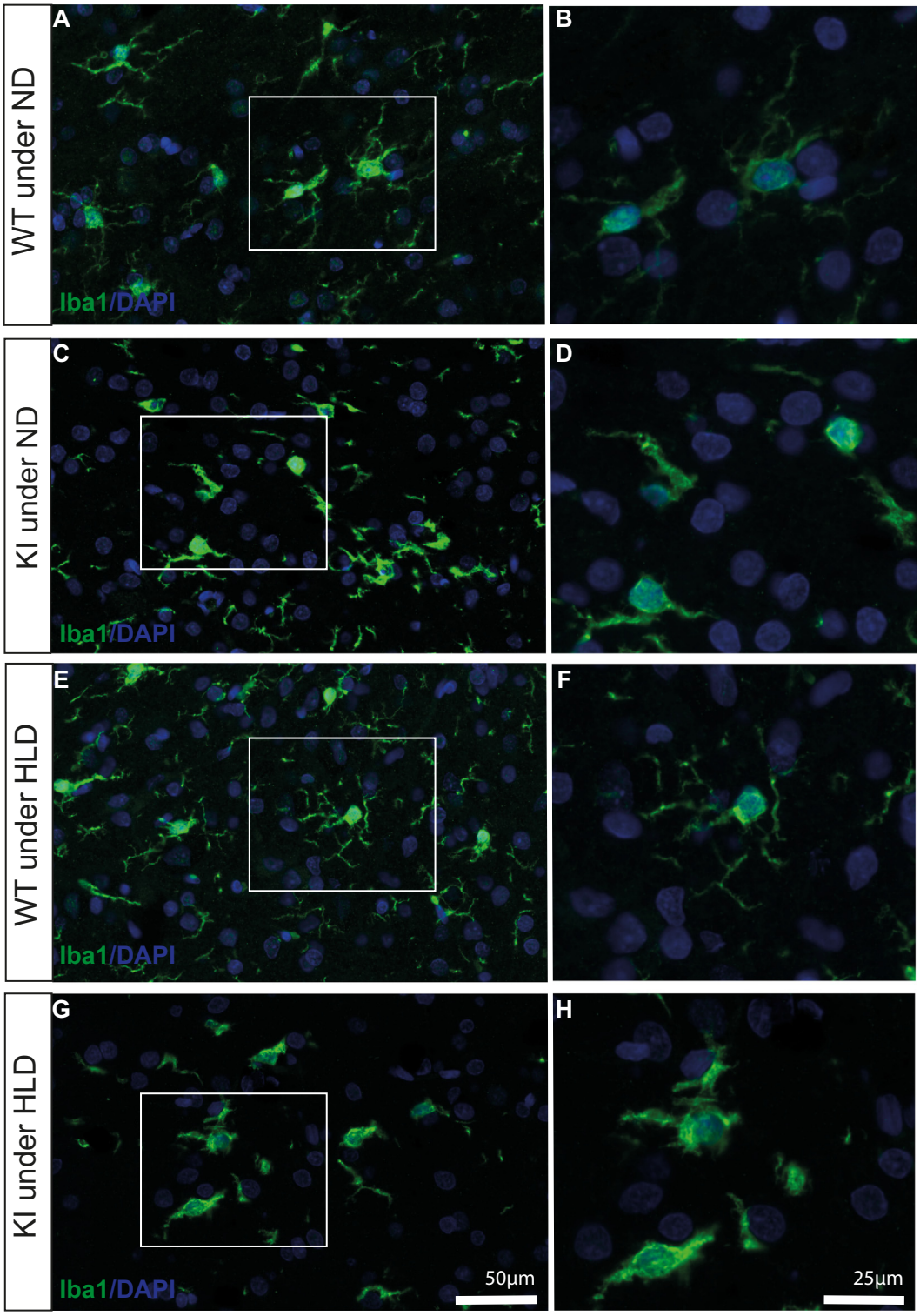

Fig. 8. Immunofluorescence staining for Iba1 in cerebellum. Representative images of Iba1 staining (**green**) in cerebellar nuclei of 6-week-old WT rats under ND (**A and B**), *Gcdh*$^{ki/ki}$ (KI) rats under ND (**C and D**), WT rats under HLD (**E and F**) and *Gcdh*$^{ki/ki}$ (KI) rats under HLD (**G and H**). DAPI (4′, 6-diamidino-2-phenylindole) co-staining is shown in blue. In the left column images with smaller magnification (40×, scale bar 50 μM) and in the right column images with higher magnification (80×, scale bar 25 μM). Iba-1-immunoreactive microglia was detected in cerebellum of *Gcdh*$^{ki/ki}$ (KI) rats under ND (B) and even more pronounced under HLD showing amoeboid morphology (D). (For interpretation of the references to colour in this figure legend, the reader is referred to the web version of this article.)

to send a satiety signal [54]. In rats, diet supplementation with 5% Lys was associated with a reduction of weight gain [55]. Lysine was also described as a potent anorectic amino acid by inducing neuronal activity at the vagal afferent [56]. In *Gcdh*$^{ki/ki}$ rats, the increased Lys intake did not affect the plasma Lys/Arg ratio. However, urinary Arg excretion was increased in *Gcdh*$^{ki/ki}$ rats under HLD. This may be well explained by competition of Lys and Arg. In rats, Arg supplementation has been associated with a significant increase in food intake [55]. Arg is known to be a

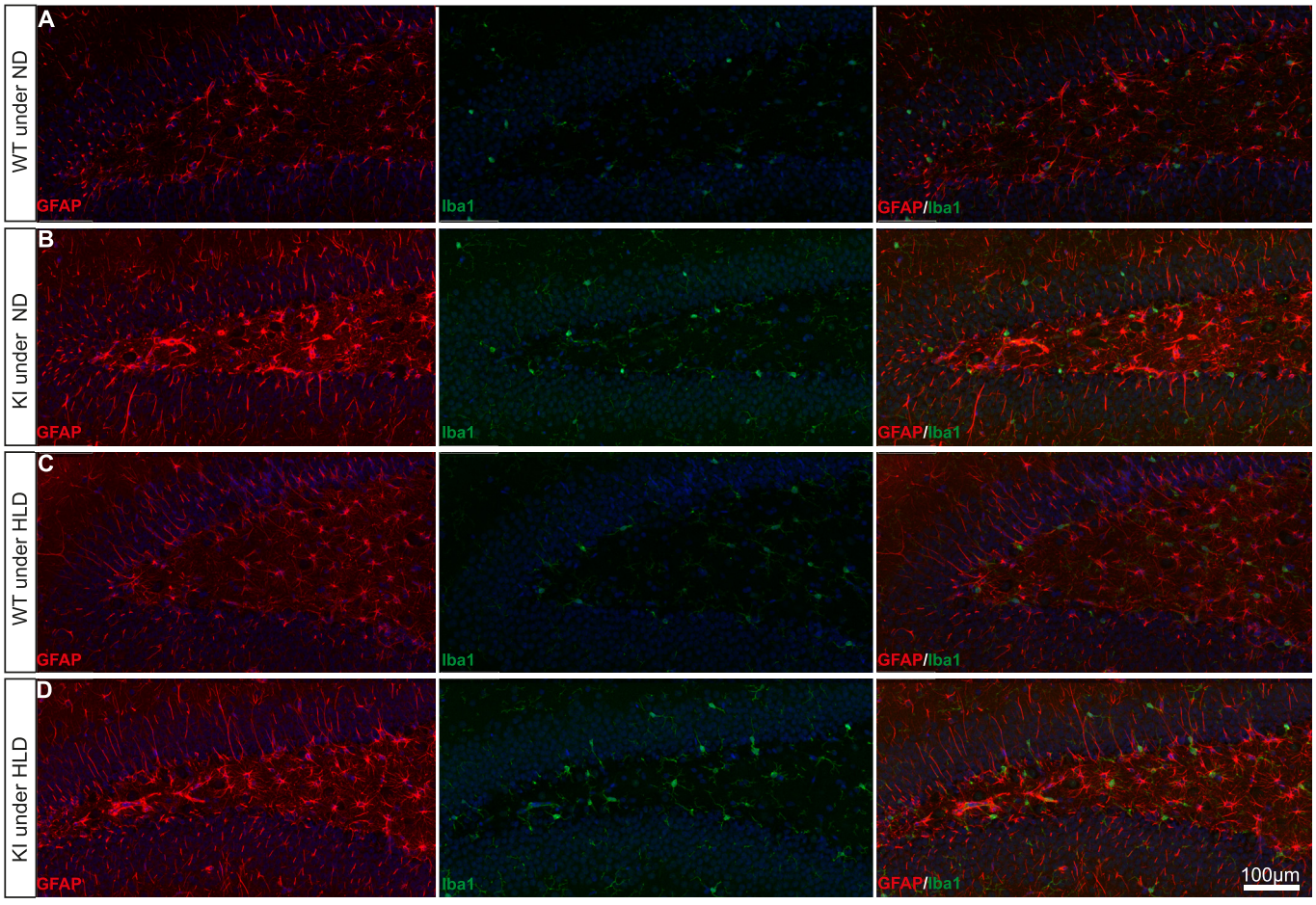

Fig. 9. Immunofluorescence staining for GFAP and Iba1 in hippocampus. Representative images of immunostaining for GFAP (**red**) and Iba1 (**green**) in hippocampus of 6-week-old WT rats under ND (**A**), *Gcdh*$^{ki/ki}$ (KI) rats under ND (**B**), WT rats under HLD (**C**) and *Gcdh*$^{ki/ki}$ (KI) rats under HLD (**D**) (Magnification 20×, scale bar 100 µM). DAPI (4′, 6-diamidino-2-phenylindole) co-staining is shown in **blue**. *Gcdh*$^{ki/ki}$ (KI) rats under ND and under HLD showed signs of astrocytic activation, which are located in the same regions as microglial activation. Scale bar 100 µM. (For interpretation of the references to colour in this figure legend, the reader is referred to the web version of this article.)

precursor of nitric oxide (modulator of food intake) [57] and inducer of growth hormone release which increases weight gain [58]. In consequence, increased Arg excretion in *Gcdh*$^{ki/ki}$ rats could affect growth hormone release and explain their low weight gain under HLD.

4.3. Increased plasma ammonium concentrations in *Gcdh*$^{ki/ki}$ rats

Hyperammonemia is not a predominant feature in patients with GA-I. *Gcdh*$^{-/-}$ mice showed increased production of urea in plasma, brain and liver, but no NH_4^+ increase in plasma [59]. The urea cycle is the final pathway for removal of excess nitrogen from the body, and the major route in mammals for NH_4^+ detoxification. The full urea cycle is only expressed in liver [61]. In contrast to *Gcdh*$^{-/-}$ mice, *Gcdh*$^{ki/ki}$ rats presented a mild, but significant increase of NH_4^+ concentrations in plasma independently of the diet. Besides this, high Arg plasma concentrations were found in both genotypes under HLD with a concomitant decrease of plasma Orn concentrations in *Gcdh*$^{ki/ki}$ rats. This constellation could indicate a potential slowdown of the urea cycle in *Gcdh*$^{ki/ki}$ rats under HLD. Recently, Lys glutarylation has been identified as new posttranslational modification in both, prokaryotic and eukaryotic cells. Proteins found to be glutarylated are involved in various cellular functions, such as translation, metabolism, and exhibited diverse subcellular localizations [62]. Tan et al. showed that carbamoyl phosphate synthetase 1 (CPS1), the rate-limiting enzyme in urea cycle, is a glutarylated protein. They demonstrated that CPS1 is targeted by SIRT5 for deglutarylation and showed that glutarylation suppresses CPS1 enzymatic activity in cell lines and *Gcdh*$^{-/-}$ mice [63]. However, analysis of CPS1 enzymatic activity in liver did not reveal any significant difference between *Gcdh*$^{ki/ki}$ and WT rats. Arginase I was also found to be glutarylated in liver of 6 week-old *Gcdh*$^{-/-}$ mice [64]. Glutarylation of arginase I might thus be the mechanism resulting in slowdown of the urea cycle, particularly in light of the increased Arg excretion in *Gcdh*$^{ki/ki}$ rats. Our observations lead to the hypothesis that under HLD the urea cycle is inhibited in *Gcdh*$^{ki/ki}$ rats and that this might be caused by glutarylation of arginase I. This observation is important for the complete understanding of the pathophysiology in GA-I and might even indicate a new therapeutic target for the treatment of GA-I.

4.4. Lysine degradation pathways in *Gcdh*$^{ki/ki}$ rats

In mammals, two Lys degradation pathways are known: the pipecolic acid and the saccharopine pathways. In the saccharopine pathway Lys is converted via a two-step transamination reaction into aminoadipic semialdehyde (AASA) by α-aminoadipic semialdehyde synthase (AASS). AASS is a bifunctional enzyme with two independent domains, the first (lysine ketoglutarate reductase) condensing Lys with α- ketoglutarate to form saccharopine, and the second (saccharopine dehydrogenase) hydrolyzing saccharopine and giving rise to glutamate and AASA/PC6 [6,8,9].

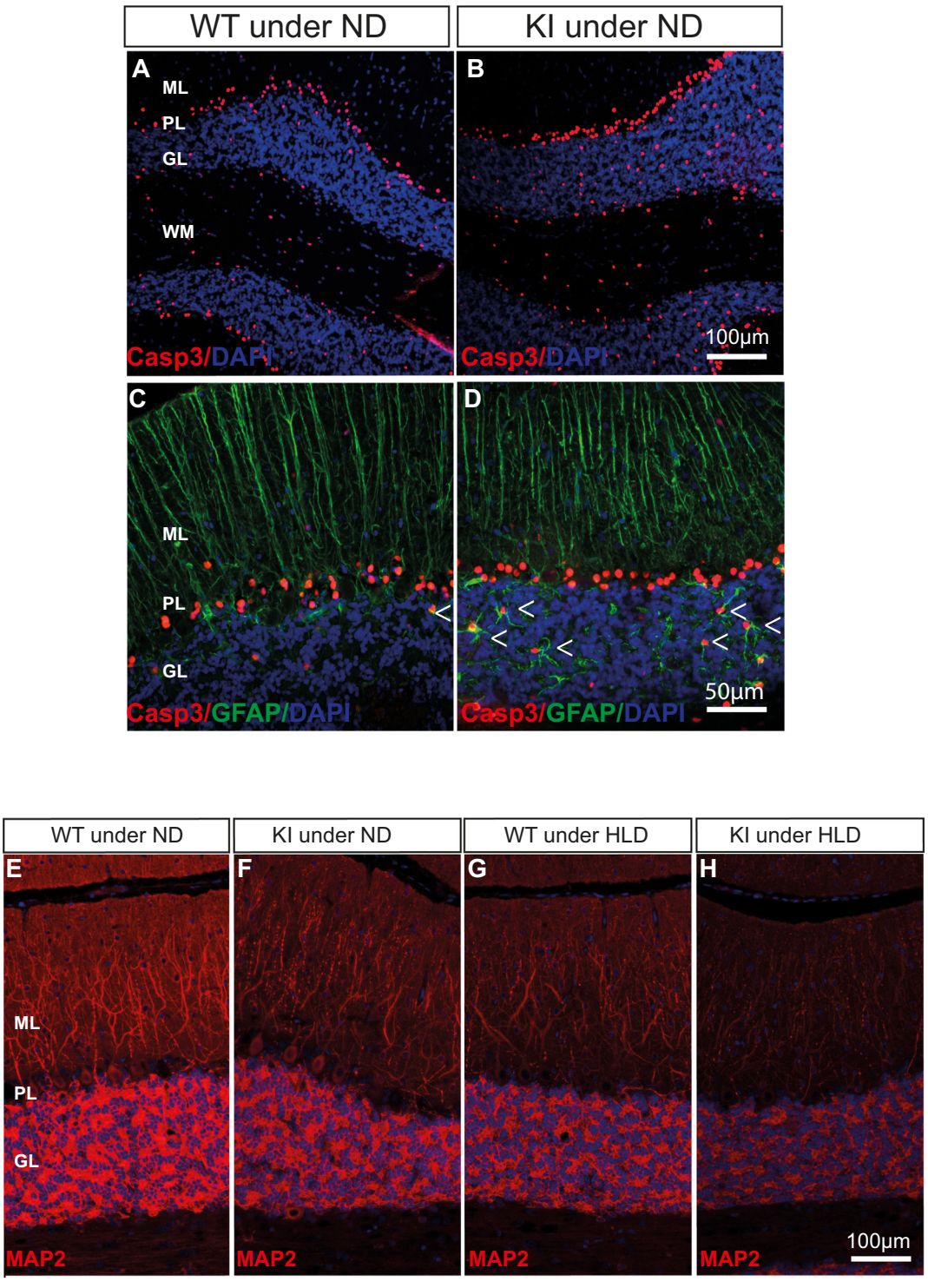

Fig. 10. Immunofluorescence staining for cleaved caspase 3, GFAP and MAP2 in cerebellum. Upper panel: Representative images of immunostaining for cleaved caspase 3 (Casp3, red) and DAPI (4′, 6-diamidino-2-phenylindole, blue) in cerebellum of 6-week-old WT rats under ND (**A**) and co-staining for GFAP (**green**) (**C**), for cleaved caspase 3 (Casp3, **red**) and DAPI (4′, 6-diamidino-2-phenylindole, **blue**) in cerebellum of 6-week-old *Gcdh*$^{ki/ki}$ (KI) rats under ND (**B**) and co-staining for GFAP (**green**) (**D**) revealed increased cell death in the granular layer (GL) and white matter (WM) of *Gcdh*$^{ki/ki}$ (KI) rats and co-localization of caspase 3 and GFAP. Molecular layer (ML), Purkinje cell layer (PL). Scale bar 100 µM for (A) and (B), 50 µM for (C) and (D). (For interpretation of the references to colour in this figure legend, the reader is referred to the web version of this article.) **Lower panel:** Representative images of immunostaining for MAP2 (**red**) in cerebellum of 6-week-old WT rats under ND (**E**), *Gcdh*$^{ki/ki}$ (KI) rats under ND (**F**), WT rats under HLD (**G**) and *Gcdh*$^{ki/ki}$ (KI) rats under HLD (**H**). DAPI (4′, 6-diamidino-2-phenylindole) staining is shown in **blue**. *Gcdh*$^{ki/ki}$ (KI) rats under HLD (H) revealed a diminished MAP2 staining in the GL and ML of cerebellum. Scale bar 100 µM.

4.4.1. Lysine degradation in periphery of Gcdh$^{ki/ki}$ rats

In plasma, Lys increased in both rat genotypes under HLD, while saccharopine concentrations were significantly lower in *Gcdh*$^{ki/ki}$ rats under HLD. We further observed a significant increase of plasmatic glutamate in WT rats under HLD, but not in *Gcdh*$^{ki/ki}$ rats. These observations indicate a potential block of the saccharopine pathway in extracerebral fluids of Gcdh$^{ki/ki}$ rats under HLD. This hypothesis was supported by a significant increase of plasmatic pipecolic acid in *Gcdh*$^{ki/ki}$

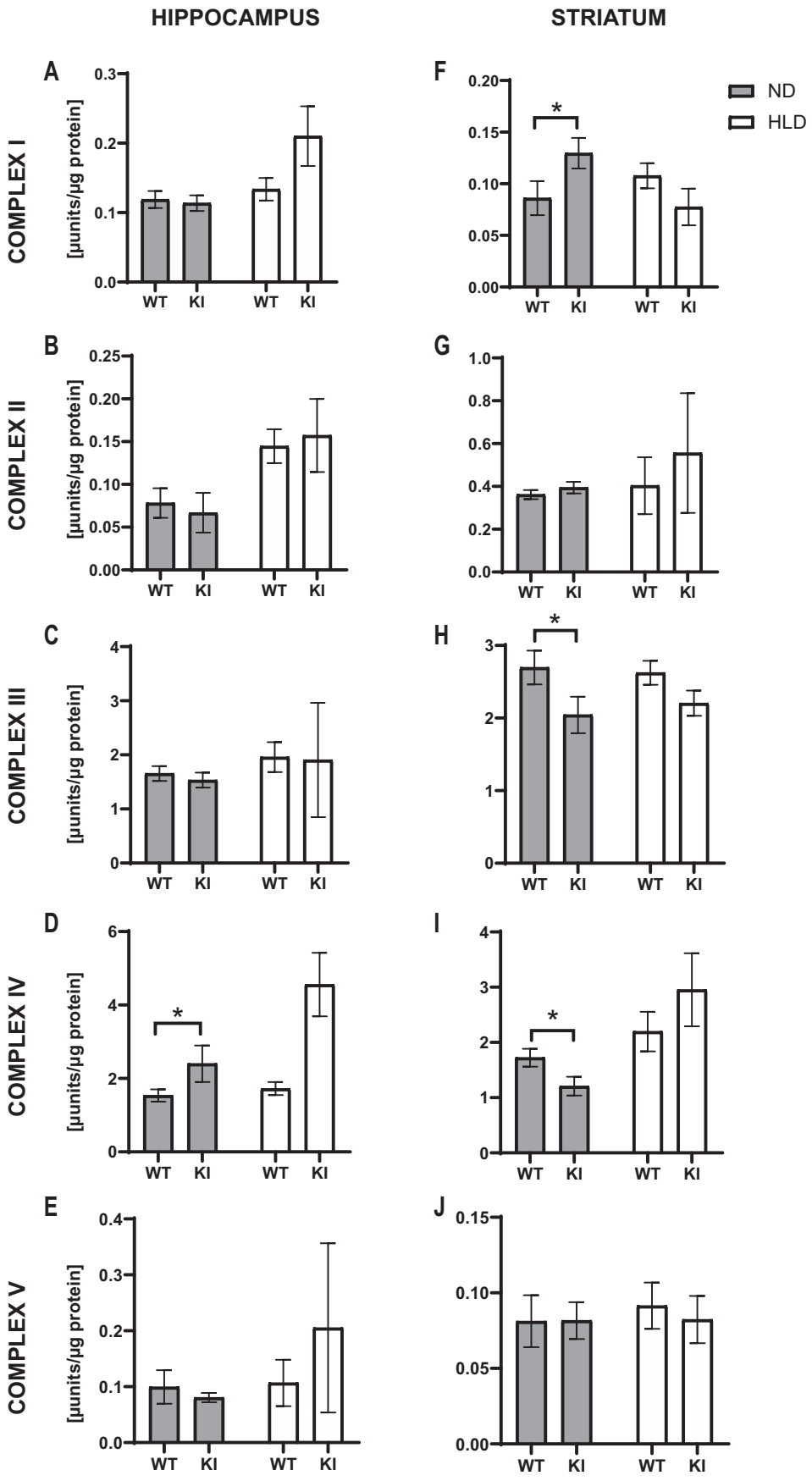
HIPPOCAMPUS
STRIATUM
ND
HLD
COMPLEX I
COMPLEX II
COMPLEX III
COMPLEX IV
COMPLEX V
[µunits/µg protein]
A
B
C
D
E
F
G
H
I
J
WT
KI
*

rats under HLD. The increased levels of plasmatic pipecolic acid in *Gcdh*$^{ki/ki}$ rats were measured as early as 24 h after start of the HLD. The observed increase of aminoadipic acid (AAA) in *Gcdh*$^{ki/ki}$ and WT rats under HLD is explained by the fact that the pipecolic acid pathway converges with the saccharopine pathway at the level of AASA. As mentioned above, protein glutarylation seems to be used as an alternative fate for utilization of glutaryl-CoA in GA-I, leading to high levels of protein glutarylation, which can result in altered activity of important metabolic enzymes [63]. The enrichment analysis of glutarylated proteins identified in liver of Gcdh$^{-/-}$ mice showed 11 genes involved in Lys degradation, which all code for enzymes of the sacharopine pathway, e.g. AASS [64]. The block of the saccharopine pathway in peripheral tissues of *Gcdh*$^{ki/ki}$ rats under HLD might be induced by glutarylation of AASS. However, double knockout *Gcdh*$^{-/-}$ *Aass*$^{-/-}$ mice showed decreased levels of GA in urine compared to single knockout *Gcdh*$^{-/-}$ mice [10], while *Gcdh*$^{ki/ki}$ rats under HLD showed significantly increased GA concentrations in urine compared to *Gcdh*$^{ki/ki}$ rats under ND. This observation does not support the hypothesis of a block of the saccharopine pathway at the level of AASS. Glutarylation of one or more other enzymes of the saccharopine pathway could explain our observations.

4.4.2. Lysine degradation in CNS of *Gcdh*$^{ki/ki}$ rats

In mouse brain, human astrocytes and a human neural progenitor cell line, the AASS-mediated pathway via saccharopine is the main route for Lys degradation. It was demonstrated that spontaneous conversion of AASA to P6C participates in pipecolic acid formation via the saccharopine pathway within the brain [11]. In striatum of *Gcdh*$^{ki/ki}$ rats under HLD, we observed a significant increase of pipecolic acid concentrations. The pipecolate pathway is not yet fully elucidated. Recently, it was observed that pipecolic acid is not only produced by α-deamination of Lys in peroxisomes, but can also be formed in mitochondria from saccharopine after ε-deamination of Lys [11]. This mechanism could explain the increased pipecolate concentrations observed in *Gcdh*$^{ki/ki}$ rats under HLD.

4.5. Structural alterations in *Gcdh*$^{ki/ki}$ rat brain

4.5.1. Microglial activation and neuroinflammation in *Gcdh*$^{ki/ki}$ rats

In *Gcdh*$^{ki/ki}$ rats, we observed microglial activation in striatum, cerebellum, hippocampus and cortex. There is now clinical and experimental evidence that astrocytes are critical regulators of CNS inflammation [66]. It is known that inflammation is an important component of the cellular response to CNS damage and disease that can significantly influence the balance between tissue loss and preservation [67]. Many brain cell types can release regulating factors of astrogliosis, including neurons, microglia, oligodendrocytes and other astrocytes [67,68]. This might be the case in *Gcdh*$^{ki/ki}$ rats, where the inflammatory process (microglial activation) seems to trigger chronic astrogliosis.

Previously, we described a significant decrease of several chemokine concentrations in organotypic brain cell 3D aggregate cultures issued from *Gcdh*$^{-/-}$ mice exposed to 10 mM Lys [32]. Proteomic analyses in striatum of *Gcdh*$^{ki/ki}$ rats showed an upregulation of Toll-interacting protein (TOLLIP) in *Gcdh*$^{ki/ki}$ rats under HLD (Suppl. Table 4). Interestingly, TOLLIP was described as an early regulator of the acute inflammatory response in the substantia nigra [69]. Both, in vitro and in vivo observations suggest that Lys overload might trigger acute neuroinflammation in GA-I.

4.5.2. Astrogliosis in *Gcdh*$^{ki/ki}$ rats

Since gliosis has been observed in post mortem brains of GA-I patients [70], several studies were performed to analyze the involvement of astrogliosis in the pathophysiology of GA-I. In addition to their multiple functions in healthy CNS, astrocytes respond to brain damage or disease with astrogliosis, which is induced, regulated or modulated by a wide variety of extracellular molecules ranging from small molecules (e.g. purines, neurotransmitters or steroid hormones) to large polypeptides (e.g. growth factors, cytokines, serum proteins or neurodegeneration molecules) [68]. In case of GA-I, the astrogliosis was associated to high Lys, 3-OHGA and GA concentrations, which induced astrocytic proliferation and caused oxidative stress [71]. While GCDH [72] and Lys degradation pathways are predominantly localized in neurons, it was demonstrated that glutarylated proteins are exclusively localized in mitochondria of glial cells [64]. Immunofluorescence staining against GFAP showed qualitative changes in *Gcdh*$^{ki/ki}$ rat astrocytes, including shorter, thicker and wavy astrocytic fibers. Astrocytic morphology in *Gcdh*$^{ki/ki}$ rats was disturbed in the same regions in which we found microglial activation (striatum, cerebellum, hippocampus and cortex), independently of the diet. The same morphological changes were observed in 3D brain cell aggregates issued from *Gcdh*$^{-/-}$ mice [32]. Astrogliosis was accompanied by astroglial scars in *Gcdh*$^{ki/ki}$ rat brains. Astroglial scars were described as derived almost entirely from newly proliferated astrocytes with a densely overlapping process that forms borders to damaged tissue and inflammation [67,73].

4.5.3. Apoptotic cell death of astrocytes and increased number of vacuoles in *Gcdh*$^{ki/ki}$ rat brain

Compared to WT rats, *Gcdh*$^{ki/ki}$ rats presented a higher number of empty vacuoles already at 6 weeks of age in several brain regions (corpus callosum and fornix, commissural nucleus, cerebellum). Luxol staining showed that these vacuoles were located in myelinated structures. Similar observations were made in white matter regions in the brain of GA-I patients and *Gcdh*$^{-/-}$ mice [22,59,65]. The increased apoptosis of astrocytes in the granular layer and white matter of *Gcdh*$^{ki/ki}$ cerebellum under ND could indicate the beginning of the formation of these vacuoles.

4.6. Excitotoxicity and altered inhibitory neurotransmission in *Gcdh*$^{ki/ki}$ rats

Disturbances of the glutamatergic and GABAergic systems have been demonstrated in the brain of *Gcdh*$^{-/-}$ mice, indicating that excitotoxicity may be involved in the neuropathology of GA-I [23]. However, metabolomics and spectroscopy analyses in striatum of *Gcdh*$^{ki/ki}$ rats did not reveal any changes in GABA and only mild changes in Glu and Gln concentrations. GO analyses of *Gcdh*$^{ki/ki}$ rats showed protein changes highly associated with synapses, including pre- and post-synaptic processes in samples from whole brain and striatum. As previously described in *Gcdh*$^{-/-}$ mice, disturbances of glutamatergic synapses could be associated with the observed proteome changes in the striatum of *Gcdh*$^{ki/ki}$ rats under ND, as confirmed by bioinformatics characterization. Synapse impairment was observed in postmortem brain studies of GA-I patients and in *Gcdh*$^{-/-}$ mice that showed a reduced number of striatal medium spiny neurons [65]. In this study, we showed a diminished MAP2 staining of cerebellar dendrites in the granular and molecular layer suggesting an impairment of glutamatergic post-synapses. These findings support the hypothesis of impairment of excitatory and inhibitory neurotransmission in GA-I.

Fig. 11. OXPHOS enzymatic activities in brain. Quantitative analyses of the enzymatic activities of the different OXPHOS complexes in hippocampus and striatum of 6-week-old WT and *Gcdh*$^{ki/ki}$ (KI) rats under ND and HLD (n = 4 for each condition). **Hippocampus:** complex I (**A**), complex II (**B**), complex III (**C**), complex IV (**D**), complex V (**E**). **Striatum:** complex I (**F**), complex II (**G**), complex III (**H**), complex IV (**I**), complex V (**J**). X-axes show genotype, y-axes show μunits/μg protein. Data shown as mean ± SD; multiple comparisons Mann Whitney: *$p < 0.05$, **$p < 0.01$, ***$p < 0.001$ after Kruskal Wallis analysis. Significant changes were only observed in *Gcdh*$^{ki/ki}$ (KI) rats under ND: In hippocampus, the activity of complex IV (cytochrome *c* oxidase) increased (D). In striatum, the activity of complex I (NADH:ubiquinone oxidoreductase) was found increased (F), while activities of complexes III (cytochrome *c* reductase) and IV (cytochrome *c* oxidase) were decreased (H–I).

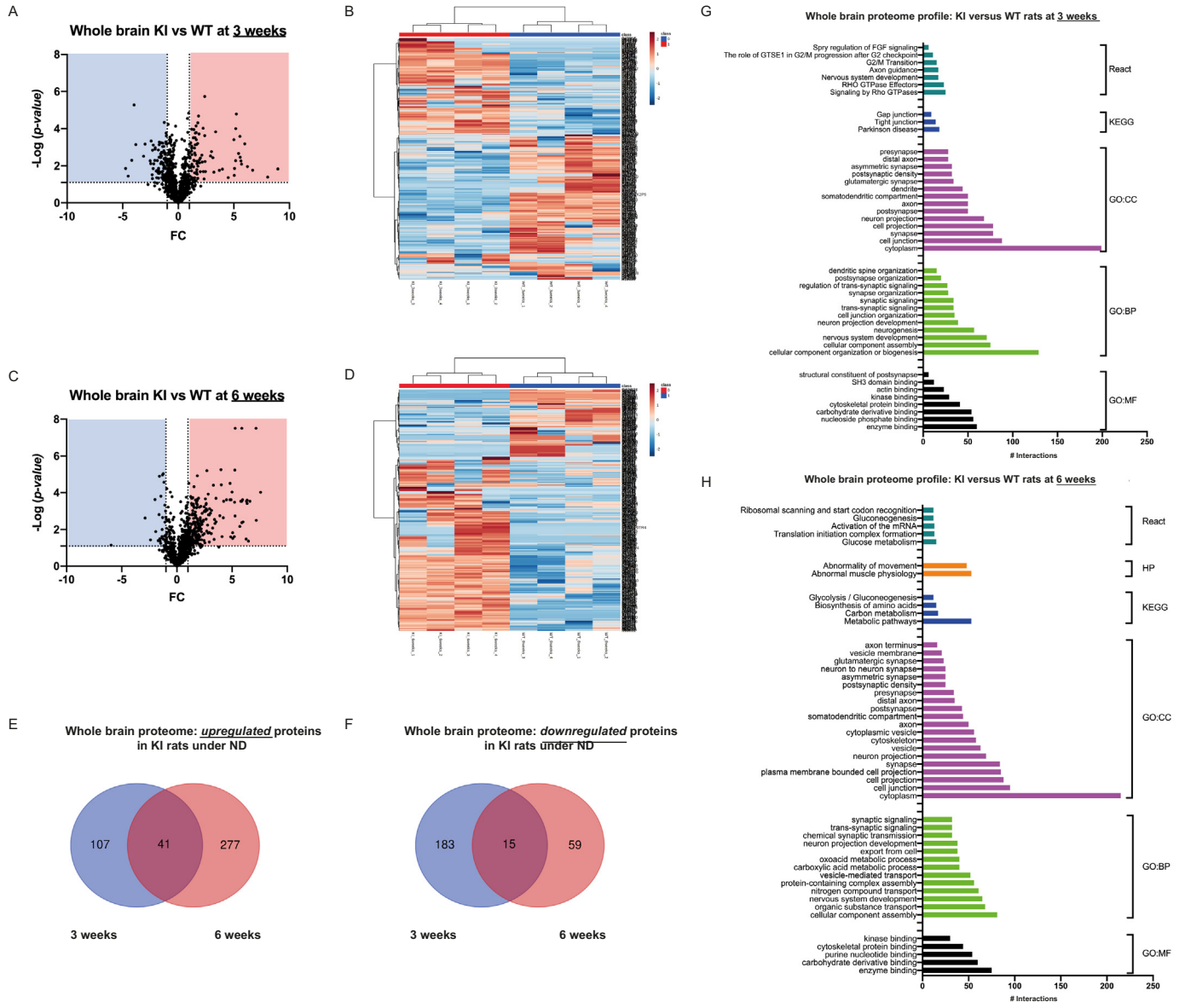

Fig. 12. Quantitative differential proteome and functional clusterization of *Gcdh*$^{ki/ki}$ rat whole brain. The proteome distribution of *Gcdh*$^{ki/ki}$ (KI) and WT rat whole brains at 3 weeks (**A**) and 6 weeks (**C**), was obtained in the volcano plot by plotting the log2 of protein abundance ratio (FC) between *Gcdh*$^{kiki/}$ and WT rats (x-axis) against the statistical significance as -Log *p*-value (y-axis). Blue and red rectangles represent the statistically significant down- and up-regulated proteins, respectively. Hierarchical clustering analyses and heat maps of protein intensities expressed as NSAF quantitative parameter were reported for *Gcdh*$^{ki/ki}$ (KI) and WT rats at 3 weeks (**B**) and 6 weeks (**D**). The colour code in the heat map represents the relative protein abundance: red and blue colour means increased and decreased protein intensity, respectively, in *Gcdh*$^{ki/ki}$ (KI) rats compared to WT rats. Venn diagrams of up-regulated (**E**) and down-regulated (**F**) proteins in *Gcdh*$^{ki/ki}$ (KI) whole brain proteome showed 41 more abundant and 15 less abundant proteins in common between 3-week-old and 6-week-old *Gcdh*$^{ki/ki}$ (KI) rats under ND. The functional clusterization of the dysregulated proteins in the whole brain of *Gcdh*$^{ki/ki}$ rats at 3 weeks (**G**) and 6 weeks (**H**) under ND was performed according to HP (Human Phenotype Ontology), KEGG (Kyoto Encyclopedia of Genes and Genomes), Gene Ontology (GO), CC (Cellular Component), GO BP (Biological Process), GO MF (Molecular Function), and React (Reactome) databases using the g: Profiler software. Enriched pathways (y-axis) were listed according to enriched values, expressed as number of involved proteins (n. intersections) (x-axis) from the *Gcdh*$^{ki/ki}$ proteome datasets. (For interpretation of the references to colour in this figure legend, the reader is referred to the web version of this article.)

4.7. Changes of brain metabolism in Gcdh$^{ki/ki}$ *rats*

4.7.1. Intracerebral depletion of free carnitine in Gcdh$^{ki/ki}$ *rats*

Our results showed increased GA and 3-OHGA concentrations in striatum, but not in CSF of *Gcdh*$^{ki/ki}$ rats under HLD. This let us suppose that these metabolites stay accumulated in the intracellular compartment of the striatum of *Gcdh*$^{ki/ki}$ rats under metabolic stress. Interestingly, C0 concentrations were only found decreased in striatal tissue and urine (and not in plasma or CSF) with a concomitant increase of C5DC concentrations. Thus, C0 seems to be exhausted by intracellular detoxification of GA and 3-OHGA without any visible C0 deficiency in the periphery. This observation supports the use of carnitine supplementation in the treatment of GA-I patients [74].

4.7.2. Intracerebral trapping of toxic metabolites in Gcdh$^{ki/ki}$ *rats*

While in periphery the accumulating Lys under HLD is eliminated by urine, the observed Lys increase in the striatum does not result in an increased Lys concentration in the CSF. Thus, Lys, GA and 3OHGA seem to be trapped intracellularly in the striatum, which could be the trigger for the different observed destructive mechanisms. Cerebral accumulation and entrapment of dicarboxylic acids have been described to be the consequence of low capacity for export of these metabolites across the blood-brain barrier [1,75,76]. The removal of soluble waste from the brain occurs via various overlapping clearance systems, which can be classified according to the compartment from and into which the waste is directly cleared. Protein and various metabolic wastes can be cleared from the intracellular and extracellular (interstitial and

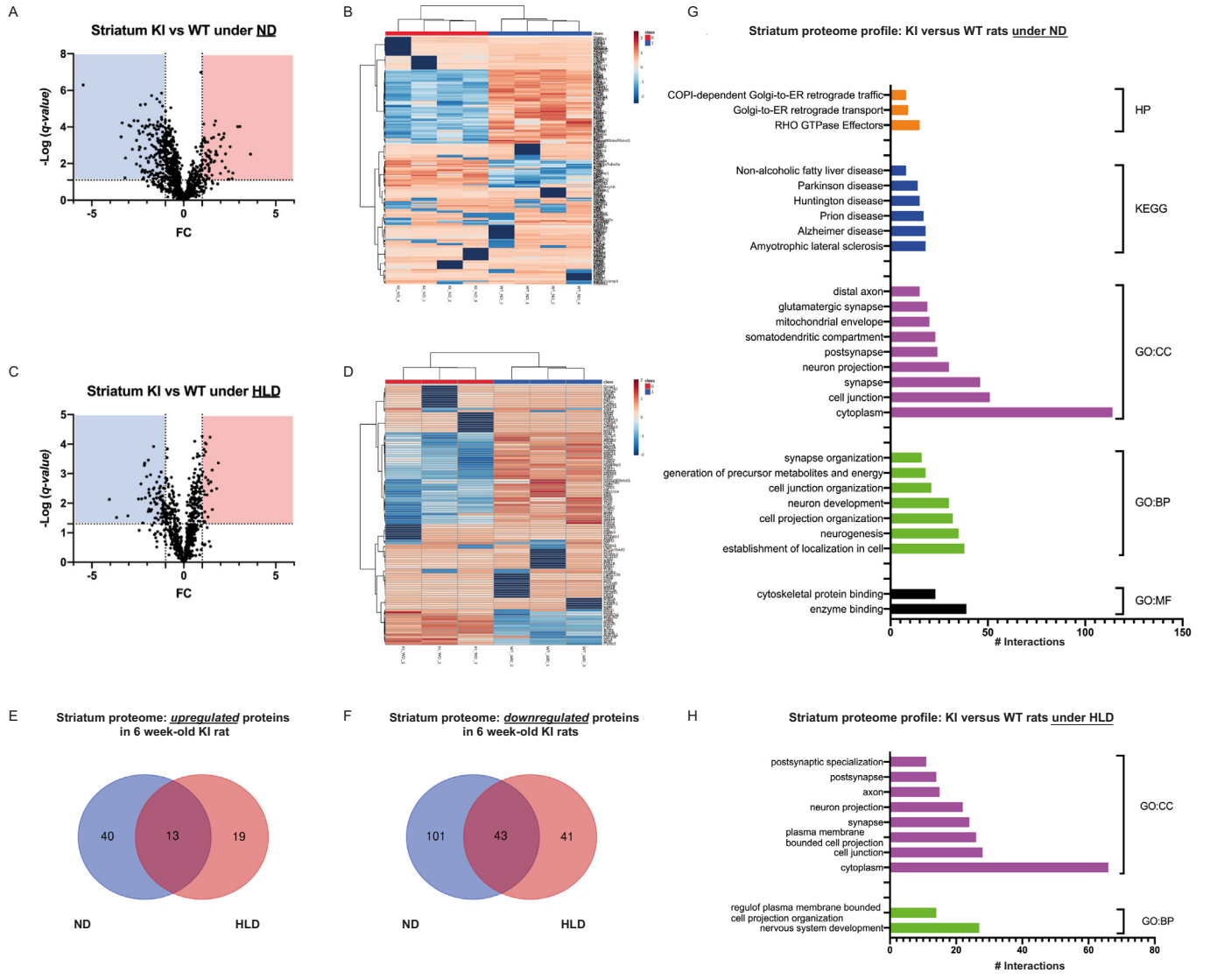

Fig. 13. Quantitative differential proteome and functional clusterization of *Gcdh*$^{ki/ki}$ rat striatum. The proteome distribution of *Gcdh*$^{ki/ki}$ (KI) and WT rat striatum at 6 weeks under ND (**A**) and HLD (**C**) was obtained in the volcano plot by plotting the log2 of protein abundance ratio (FC) between *Gcdh*$^{kiki/}$ and WT rats (x-axis) against the statistical significance as -Log p-value (y-axis). Blue and red rectangles represent the statistically significant down- and up-regulated proteins, respectively. Hierarchical clustering analyses and heat maps of protein abundances expressed by LFQ intensities were reported for *Gcdh*$^{ki/ki}$ (KI) and WT rats under ND (**B**) and HLD (**D**). The colour code in the heat map represents the relative protein abundance: red and blue colour means increased and decreased protein intensity, respectively, in *Gcdh*$^{ki/ki}$ (KI) rats compared to WT rats. Venn diagrams of up-regulated (**E**) and down-regulated (**F**) proteins in *Gcdh*$^{ki/ki}$ (KI) striatum proteome showed 13 more abundant and 43 less abundant proteins in common between 6-week-old *Gcdh*$^{ki/ki}$ (KI) rats under ND and HLD. The functional clusterization of the dysregulated proteins in the striatum of *Gcdh*$^{ki/ki}$ rats at 6 weeks under ND (**G**) and HLD (**H**) was performed according to HP (Human Phenotype Ontology), KEGG (Kyoto Encyclopedia of Genes and Genomes), Gene Ontology (GO), CC (Cellular Component), GO BP (Biological Process), GO MF (Molecular Function), and React (Reactome) databases using the g: Profiler software. Enriched pathways (y-axis) were listed according to enriched values, expressed as number of involved proteins (n. intersections) (x-axis) from the *Gcdh*$^{ki/ki}$ proteome datasets. (For interpretation of the references to colour in this figure legend, the reader is referred to the web version of this article.)

cerebrospinal fluids) compartments. These proteins or metabolites can then be removed by enzymatic degradation or cellular uptake, exported into the blood or lymph, or recirculated in the CSF [54,77,78]. Clearance systems are poorly studied in the brain and could be an important area for future research in GA-I pathology. The existing ways for waste clearance in brain might be suitable therapeutic targets in GA-I and other diseases with enzymatic blocks that lead to cerebral accumulation of toxic substances.

4.7.3. Imbalance of intra- and extracellular creatine concentrations and osmotic stress in Gcdh$^{ki/ki}$ *rats under HLD*

Apart of its well-known function in energy metabolism for ATP regeneration through the creatine/phosphocreatine/creatine kinase system, creatine has many functions in the brain. It is one of the main CNS osmolites and was found to act as antioxidant and probably also as neurotransmitter. Under HLD, creatine concentrations in CSF of *Gcdh*$^{ki/ki}$ rats were significantly lower than in WT rats. In contrast, creatine concentrations measured in brain tissue of striatum were found to be higher in *Gcdh*$^{ki/ki}$ rats compared to WT rats under HLD. This indicates that under HLD creatine was retained intracellularly in striatum of *Gcdh*$^{ki/ki}$ rats, where it might serve for energy supply or as antioxidant. As creatine has an important osmotic action, intracellular creatine trapping in striatum of *Gcdh*$^{ki/ki}$ rats might lead to imbalances of cell volume homeostasis and osmotic stress. A decrease of myo-inositol in brain 1H-MRS has recently been identified as an early sign of osmotic stress in an animal model for type C hepatic encephalopathy [35]. We observed a decrease of myo-inositol in striatum of 6-week-old *Gcdh*$^{ki/ki}$ rats under HLD by 1H-MRS. This observation further supports the hypothesis of osmotic stress in brain of *Gcdh*$^{ki/ki}$ rats under HLD.

4.7.4. Intracerebral NH_4^+ accumulation in $Gcdh^{ki/ki}$ rats

We previously showed a significant increase of NH_4^+ concentrations in culture media of 3D organotypic WT brain cell aggregates exposed to GA and 3-OHGA as well as in 3D organotypic brain cell cultures derived from $Gcdh^{-/-}$ mice exposed to 10 mM Lys [32,60]. MR spectroscopy of striatum showed a significant decrease of Gln concentrations in $Gcdh^{ki/ki}$ rats under ND with a tendency to decrease in striatal tissue under the same condition. In parallel, we found a significant downregulation of glutamine synthetase by proteomics analyses in whole brains of $Gcdh^{ki/ki}$ rats under ND. Glutamine synthetase is expressed in astrocytes and plays a central role in the metabolic regulation of the neurotransmitter glutamate and the detoxification of brain NH_4^+ [79]. Apoptotic cell death of astrocytes might lead to the observed downregulation of glutamine synthetase, in turn provoking intracerebral accumulation of NH_4^+. These results together with our previous observations point to the hypothesis that intracerebral NH_4^+ accumulation plays a crucial role in the neuropathogenesis of GA-I. Better methods need to be developed for measurements of NH_4^+ concentrations in brain tissues of $Gcdh^{ki/ki}$ rats.

4.8. Impaired OXPHOS activities in $Gcdh^{ki/ki}$ rat brain

Disturbed mitochondrial function has been associated to brain injury in GA-I [80,81]. Several studies in $Gcdh^{-/-}$ mice showed different bioenergetics dysfunctions as depletion of ATP, phosphocreatine, coenzyme A and decrease of citric acid cycle activities [24,59,82–84]. Our analyses of the respiratory chain in brain of $Gcdh^{ki/ki}$ rats under ND did not only reveal changes in striatum as previously described in other GA-I models, but also in hippocampus. In striatum, we observed an inhibition of complex IV as described in $Gcdh^{-/-}$ mice after intrastriatal injection with quinolinic acid [82] and in patients [85]. Proteomics analyses in striatum of $Gcdh^{ki/ki}$ rats under ND supported this result with a significant downregulation of cytochrome *c* oxidase subunit 4 isoform 1 (Cox4i1) and cytochrome *c* oxidase subunit 6c-2 (Cox6c2). Complexes I and III also showed a decreased enzymatic activity in striatum of $Gcdh^{ki/ki}$ rats under ND. Both findings could be correlated with proteomics findings. For complex I, NADH dehydrogenase [ubiquinone] iron-sulfur protein 4 (Ndufs4) and NADH dehydrogenase [ubiquinone] iron-sulfur protein 6 (Ndufs6) were observed downregulated in $Gcdh^{ki/ki}$ rats under ND. For complex III, cytochrome *b*-c1 complex subunit 8 (Uqcrq) was observed downregulated in brain of $Gcdh^{ki/ki}$ rats under ND. Oxidative stress in hippocampus of GA-I patients or animal models has never been described before. However, in hippocampus of $Gcdh^{ki/ki}$ rats under ND, we observed a significant increase of the enzymatic activity of complex IV. This finding might be important in relation to the described learning disabilities in GA-I patients [16].

4.8.1. Advantages of the $Gcdh^{ki/ki}$ rat model

As $Gcdh^{-/-}$ mice, our new rat model for GA-I recapitulates most of the biochemical and clinical features observed in patients with GA-I. In comparison to $Gcdh^{-/-}$ mice, our rat model has significant advantages: It carries the most frequent mutation of the Caucasian population, which allows therapeutic studies for the use of small molecules (e.g. chaperones) to restore enzymatic activities, which might thus open new therapeutic perspectives. Particularly for diseases affecting the brain, rat models have several advantages compared to mouse models: Rats have larger brains (relevant for imaging) and a higher CSF volume (important for the number of possible measurements). Rat metabolism is closer to human and a wider range of behavioral tests have been established and validated in rats [86].

5. Conclusions

We successfully created the first rat model for GA-I carrying the most frequent point mutation of the Caucasian population. This knock-in rat model is viable, reproductive and has a high excretor phenotype. As $Gcdh^{-/-}$ mice, $Gcdh^{ki/ki}$ rats do not present any spontaneous AEC, but metabolic stress can be triggered by HLD. Lys overload by HLD led to interesting observations on Lys degradation pathways in periphery and brain of $Gcdh^{ki/ki}$ rats. We confirmed several known aspects and uncovered additional relevant features of (neuro-) pathogenesis in GA-I.

We found further evidence for the hypothesis that cerebral NH_4^+ accumulation might play a crucial role in brain damage of GA-I patients: It seems that intracellular trapping of toxic metabolites, excitotoxicity and energy failure might trigger microglial activation, which leads to neuroinflammation and astrogliosis. This might result in apoptotic cell death of astrocytes that becomes microscopically visible in form of brain vacuoles. Astrocytic loss could then lead to downregulation of glutamine synthetase which might be the key mechanism resulting in diminished Gln concentrations and cerebral NH_4^+ accumulation.

We conclude that our rat model for GA-I is a suitable model not only for the study of different aspect of the disease-specific pathophysiology, but also for the development of new therapeutic strategies in GA-I as well as the study of lysine degradation pathways in brain and periphery.

Funding

This project was supported by the Swiss National Science Foundation (http://www.snf.ch) grant number 310030–127497 and by an unrestricted research grant of Sanofi Genzyme given to D. Ballhausen.

CPS1 enzymatic activity measurements were supported by the Swiss National Science Foundation grant number 320030–176088 given to J. Häberle.

Acknowledgements

We thank Marc Loup (lab technician, research group of O. Braissant), Annaelle Williamoz and Tayanne Marques (lab technician students from Ecole superior de la santé de Lausanne) as well as Michael Dupertuis (chief lab technician, Service of clinical chemistry) for technical assistance, Myriam Vuillet (animal facility of the CHUV), Mario Lepore, Da Silva Analina Raquel and Valentine Bressoud (animal facility of the EPFL) for animal care and technical assistance. Proton magnetic resonance spectroscopy (1H-MRS) of CNS at high magnetic field (9.4 T) was made possible thanks to the CIBM Center for Biomedical Imaging, a Swiss research center of excellence founded and supported by Lausanne University Hospital (CHUV), University of Lausanne (UNIL), Ecole Polytechnique Fédérale de Lausanne (EPFL), University of Geneva (UNIGE) and Geneva University Hospitals (HUG).

Appendix A. Supplementary data

Supplementary data to this article can be found online at https://doi.org/10.1016/j.ymgme.2021.03.017.

References

[1] S.W. Sauer, J.G. Okun, G. Fricker, A. Mahringer, I. Muller, L.R. Crnic, et al., Intracerebral accumulation of glutaric and 3-hydroxyglutaric acids secondary to limited flux across the blood-brain barrier constitute a biochemical risk factor for neurodegeneration in glutaryl-CoA dehydrogenase deficiency, J. Neurochem. 97 (2006) 899–910.

[2] K.A. Strauss, E.G. Puffenberger, D.L. Robinson, D.H. Morton, Type I glutaric aciduria, part 1: natural history of 77 patients, Am. J. Med. Genet. C: Semin. Med. Genet. 121C (2003) 38–52.

[3] N. Boy, K. Mengler, E. Thimm, K.A. Schiergens, T. Marquardt, N. Weinhold, et al., Newborn screening: a disease-changing intervention for glutaric aciduria type 1, Ann. Neurol. 83 (2018) 970–979.

[4] Y.E. Chang, Lysine metabolism in the rat brain: the pipecolic acid-forming pathway, J. Neurochem. 30 (1978) 347–354.

[5] Y.F. Chang, Lysine metabolism in the rat brain: blood-brain barrier transport, formation of pipecolic acid and human hyperpipecolatemia, J. Neurochem. 30 (1978) 355–360.

[6] A. Hallen, J.F. Jamie, A.J. Cooper, Lysine metabolism in mammalian brain: an update on the importance of recent discoveries, Amino Acids 45 (2013) 1249–1272.

[7] C. Biagosch, R.D. Ediga, S.V. Hensler, M. Faerberboeck, R. Kuehn, W. Wurst, et al., Elevated glutaric acid levels in Dhtkd1−/Gcdh- double knockout mice challenge our current understanding of lysine metabolism, Biochim. Biophys. Acta Mol. basis Dis. 2017 (1863) 2220–2228.
[8] L.M. Crowther, D. Mathis, M. Poms, B. Plecko, New insights into human lysine degradation pathways with relevance to pyridoxine-dependent epilepsy due to antiquitin deficiency, J. Inherit. Metab. Dis. 42 (2019) 620–628.
[9] I.A. Pena, L.A. Marques, A.B. Laranjeira, J.A. Yunes, M.N. Eberlin, A. MacKenzie, et al., Mouse lysine catabolism to aminoadipate occurs primarily through the saccharopine pathway; implications for pyridoxine dependent epilepsy (PDE), Biochim. Biophys. Acta Mol. basis Dis. 2017 (1863) 121–128.
[10] J. Leandro, T. Dodatko, R.J. DeVita, H. Chen, B. Stauffer, C. Yu, et al., Deletion of 2-aminoadipic semialdehyde synthase limits metabolite accumulation in cell and mouse models for glutaric aciduria type 1, J. Inherit. Metab. Dis. 43 (2020) 1154–1164.
[11] J. Leandro, S.M. Houten, The lysine degradation pathway: subcellular compartmentalization and enzyme deficiencies, Mol. Genet. Metab. 131 (2020) 14–22.
[12] G.F. Hoffmann, W. Meier-Augenstein, S. Stockler, R. Surtees, D. Rating, W.L. Nyhan, Physiology and pathophysiology of organic acids in cerebrospinal fluid, J. Inherit. Metab. Dis. 16 (1993) 648–669.
[13] S.K. Lin, S.G. Hsu, E.S. Ho, C.R. Tsai, Y.T. Hseih, F.C. Lo, et al., Glutaric aciduria (type I): prenatal ultrasonographic findings, Ultrasound Obstet. Gynecol. 20 (2002) 305–307.
[14] C. Mellerio, S. Marignier, P. Roth, P. Gaucherand, V. Des Portes, J.P. Pracros, et al., Prenatal cerebral ultrasound and MRI findings in glutaric aciduria Type 1: a de novo case, Ultrasound Obstet. Gynecol. 31 (2008) 712–714.
[15] R. Forstner, G.F. Hoffmann, I. Gassner, P. Heideman, J.B. De Klerk, B. Lawrenz-Wolf, et al., Glutaric aciduria type I: ultrasonographic demonstration of early signs, Pediatr. Radiol. 29 (1999) 138–143.
[16] N. Boy, C. Muhlhausen, E.M. Maier, J. Heringer, B. Assmann, P. Burgard, et al., Proposed recommendations for diagnosing and managing individuals with glutaric aciduria type I: second revision, J. Inherit. Metab. Dis. 40 (2017) 75–101.
[17] E. Neumaier-Probst, I. Harting, A. Seitz, C. Ding, S. Kolker, Neuroradiological findings in glutaric aciduria type I (glutaryl-CoA dehydrogenase deficiency), J. Inherit. Metab. Dis. 27 (2004) 869–876.
[18] M.H. Beauchamp, A. Boneh, V. Anderson, Cognitive, behavioural and adaptive profiles of children with glutaric aciduria type I detected through newborn screening, J. Inherit. Metab. Dis. (Suppl 1) (2009) S207–S213.
[19] N. Boy, S.F. Garbade, J. Heringer, A. Seitz, S. Kolker, I. Harting, Patterns, evolution, and severity of striatal injury in insidious- vs acute-onset glutaric aciduria type 1, J. Inherit. Metab. Dis. 42 (2019) 117–127.
[20] N. Boy, J. Heringer, R. Brackmann, O. Bodamer, A. Seitz, S. Kolker, et al., Extrastriatal changes in patients with late-onset glutaric aciduria type I highlight the risk of long-term neurotoxicity, Orphanet J Rare Dis. 12 (2017) 77.
[21] I. Harting, N. Boy, J. Heringer, A. Seitz, M. Bendszus, P.J. Pouwels, et al., (1)H-MRS in glutaric aciduria type 1: impact of biochemical phenotype and age on the cerebral accumulation of neurotoxic metabolites, J. Inherit. Metab. Dis. 38 (2015) 829–838.
[22] D.M. Koeller, M. Woontner, L.S. Crnic, B. Kleinschmidt-DeMasters, J. Stephens, E.L. Hunt, et al., Biochemical, pathologic and behavioral analysis of a mouse model of glutaric acidemia type I, Hum. Mol. Genet. 11 (2002) 347–357.
[23] M. Wajner, A.U. Amaral, G. Leipnitz, B. Seminotti, Pathogenesis of brain damage in glutaric acidemia type I: lessons from the genetic mice model, Int. J. Dev. Neurosci. 78 (2019) 215–221.
[24] A.U. Amaral, C. Cecatto, B. Seminotti, C.A. Ribeiro, V.L. Lagranha, C.C. Pereira, et al., Experimental evidence that bioenergetics disruption is not mainly involved in the brain injury of glutaryl-CoA dehydrogenase deficient mice submitted to lysine overload, Brain Res. 2015 (1620) 116–129.
[25] D.M. Koeller, S. Sauer, M. Wajner, C.F. de Mello, S.I. Goodman, M. Woontner, et al., Animal models for glutaryl-CoA dehydrogenase deficiency, J. Inherit. Metab. Dis. 27 (2004) 813–818.
[26] W.J. Zinnanti, J. Lazovic, Mouse model of encephalopathy and novel treatment strategies with substrate competition in glutaric aciduria type I, Mol. Genet. Metab. 100 (Suppl. 1) (2010) S88–S91.
[27] B. Keyser, C. Muhlhausen, A. Dickmanns, E. Christensen, N. Muschol, K. Ullrich, et al., Disease-causing missense mutations affect enzymatic activity, stability and oligomerization of glutaryl-CoA dehydrogenase (GCDH), Hum. Mol. Genet. 17 (2008) 3854–3863.
[28] S.I. Goodman, D.E. Stein, S. Schlesinger, E. Christensen, M. Schwartz, C.R. Greenberg, et al., Glutaryl-CoA dehydrogenase mutations in glutaric acidemia (type I): review and report of thirty novel mutations, Hum. Mutat. 12 (1998) 141–144.
[29] M. Schwartz, E. Christensen, A. Superti-Furga, N.J. Brandt, The human glutaryl-CoA dehydrogenase gene: report of intronic sequences and of 13 novel mutations causing glutaric aciduria type I, Hum. Genet. 102 (1998) 452–458.
[30] E. Christensen, A. Ribes, B. Merinero, J. Zschocke, Correlation of genotype and phenotype in glutaryl-CoA dehydrogenase deficiency, J. Inherit. Metab. Dis. 27 (2004) 861–868.
[31] S. Zhao, J. Shetty, L. Hou, A. Delcher, B. Zhu, K. Osoegawa, et al., Human, mouse, and rat genome large-scale rearrangements: stability versus speciation, Genome Res. 14 (2004) 1851–1860.
[32] H.P. Cudré-Cung, N. Remacle, S. do Vale-Pereira, M. Gonzalez, H. Henry, J. Ivanisevic, et al., Ammonium accumulation and chemokine decrease in culture media of Gcdh (−/−) 3D reaggregated brain cell cultures, Mol. Genet. Metab. 126 (2019) 416–428.
[33] T. Teav, H. Gallart-Ayala, V. van der Velpen, F. Mehl, H. Henry, J. Ivanisevic, Merged targeted quantification and untargeted profiling for comprehensive assessment of Acylcarnitine and amino acid metabolism, Anal. Chem. 91 (2019) 11757–11769.
[34] S. Pekkala, A.I. Martínez, B. Barcelona, J. Gallego, E. Bendala, I. Yefimenko, et al., Structural insight on the control of urea synthesis: identification of the binding site for N-acetyl-L-glutamate, the essential allosteric activator of mitochondrial carbamoyl phosphate synthetase, Biochem. J. 424 (2009) 211–220.
[35] O. Braissant, V. Rackayová, K. Pierzchala, J. Grosse, V.A. McLin, C. Cudalbu, Longitudinal neurometabolic changes in the hippocampus of a rat model of chronic hepatic encephalopathy, J. Hepatol. 71 (2019) 505–515.
[36] V. Mlynárik, G. Gambarota, H. Frenkel, R. Gruetter, Localized short-echo-time proton MR spectroscopy with full signal-intensity acquisition, Magn. Reson. Med. 56 (2006) 965–970.
[37] C. Cudalbu, V. Mlynárik, R. Gruetter, Handling macromolecule signals in the quantification of the neurochemical profile, J. Alzheimer's Dis. 31 (Suppl. 3) (2012) S101–S115.
[38] R.G. Feichtinger, E. Petervari, M. Zopf, S. Vidali, S. Aminzadeh-Gohari, J.A. Mayr, et al., Effects of alpha-melanocyte-stimulating hormone on mitochondrial energy metabolism in rats of different age-groups, Neuropeptides. 64 (2017) 123–130.
[39] P. Rustin, D. Chretien, T. Bourgeron, B. Gérard, A. Rötig, J.M. Saudubray, et al., Biochemical and molecular investigations in respiratory chain deficiencies, Clin. Chim. Acta; Int. J. Clin. Chem. 228 (1994) 35–51.
[40] E. Imperlini, L. Santorelli, S. Orrù, E. Scolamiero, M. Ruoppolo, M. Caterino, Mass spectrometry-based metabolomic and proteomic strategies in organic Acidemias, Biomed. Res. Int. 2016 (2016) 9210408.
[41] V. De Pasquale, M. Costanzo, R.A. Siciliano, M.F. Mazzeo, V. Pistorio, L. Bianchi, et al., Proteomic analysis of Mucopolysaccharidosis IIIB mouse brain, Biomolecules. 10 (2020).
[42] M. Costanzo, A. Cevenini, E. Marchese, E. Imperlini, M. Raia, L. Del Vecchio, et al., Label-free quantitative proteomics in a Methylmalonyl-CoA Mutase-silenced Neuroblastoma cell line, Int. J. Mol. Sci. 19 (2018).
[43] M. Caterino, M. Zacchia, M. Costanzo, G. Bruno, D. Arcaniolo, F. Trepiccione, et al., Urine proteomics revealed a significant correlation between urine-Fibronectin abundance and estimated-GFR decline in patients with Bardet-Biedl syndrome, Kidney Blood Press. Res. 43 (2018) 389–405.
[44] V. De Pasquale, M. Caterino, M. Costanzo, R. Fedele, M. Ruoppolo, L.M. Pavone, Targeted Metabolomic analysis of a Mucopolysaccharidosis IIIB mouse model reveals an imbalance of branched-chain amino acid and fatty acid metabolism, Int. J. Mol. Sci. 21 (2020).
[45] M. Costanzo, M. Caterino, A. Cevenini, V. Jung, C. Chhuon, J. Lipecka, et al., Proteomics reveals that Methylmalonyl-CoA Mutase modulates cell architecture and increases susceptibility to stress, Int. J. Mol. Sci. 21 (2020).
[46] M. Caterino, M. Ruoppolo, G.R.D. Villani, E. Marchese, M. Costanzo, G. Sotgiu, et al., Influence of sex on urinary organic acids: a cross-sectional study in children, Int. J. Mol. Sci. 21 (2020).
[47] J. Reimand, M. Kull, H. Peterson, J. Hansen, J. Vilo, g:Profiler–a web-based toolset for functional profiling of gene lists from large-scale experiments, Nucleic Acids Res. 35 (2007) W193–W200.
[48] M.V. Kurkina, S.V. Mihaylova, G.V. Baydakova, E.V. Saifullina, S.A. Korostelev, D.V. Pyankov, et al., Molecular and biochemical study of glutaric aciduria type 1 in 49 Russian families: nine novel mutations in the GCDH gene, Metab. Brain Dis. 35 (6) (2020) 1009–1016.
[49] S. Kolker, S.F. Garbade, C.R. Greenberg, J.V. Leonard, J.M. Saudubray, A. Ribes, et al., Natural history, outcome, and treatment efficacy in children and adults with glutaryl-CoA dehydrogenase deficiency, Pediatr. Res. 59 (2006) 840–847.
[50] E.M.C. Märtner, E.M. Maier, K. Mengler, E. Thimm, K.A. Schiergens, T. Marquardt, et al., Impact of interventional and non-interventional variables on anthropometric long-term development in glutaric aciduria type 1: a national prospective multi-Centre study, J. Inherit. Metab. Dis. (2020) https://doi.org/10.1002/jimd.12335.
[51] S. Sugama, S.A. Wirz, A.M. Barr, B. Conti, T. Bartfai, T. Shibasaki, Interleukin-18 null mice show diminished microglial activation and reduced dopaminergic neuron loss following acute 1-methyl-4-phenyl-1,2,3,6-tetrahydropyridine treatment, Neuroscience. 128 (2004) 451–458.
[52] I. Mori, M.J. Hossain, K. Takeda, H. Okamura, Y. Imai, S. Kohsaka, et al., Impaired microglial activation in the brain of IL-18-gene-disrupted mice after neurovirulent influenza a virus infection, Virology. 287 (2001) 163–170.
[53] C.N. Khwatenge, B.M. Kimathi, T. Taylor-Bowden, S.N. Nahashon, Expression of lysine-mediated neuropeptide hormones controlling satiety and appetite in broiler chickens, Poult. Sci. 99 (2020) 1409–1420.
[54] G. Lazutkaite, A. Soldà, K. Lossow, W. Meyerhof, N. Dale, Amino acid sensing in hypothalamic tanycytes via umami taste receptors, Mol. Metab. 6 (2017) 1480–1492.
[55] R. Ayaso, H. Ghattas, M. Abiad, O. Obeid, Meal pattern of male rats maintained on amino acid supplemented diets: the effect of tryptophan, lysine, arginine, proline and threonine, Nutrients. 6 (2014) 2509–2522.
[56] J. Jordi, B. Herzog, S.M. Camargo, C.N. Boyle, T.A. Lutz, F. Verrey, Specific amino acids inhibit food intake via the area postrema or vagal afferents, J. Physiol. 591 (2013) 5611–5621.
[57] J.E. Morley, J.F. Flood, Evidence that nitric oxide modulates food intake in mice, Life Sci. 49 (1991) 707–711.
[58] T.J. Merimee, D. Rabinowtitz, S.E. Fineberg, Arginine-initiated release of human growth hormone. Factors modifying the response in normal man, N. Engl. J. Med. 280 (1969) 1434–1438.
[59] S.W. Sauer, S. Opp, S. Komatsuzaki, A.-E. Blank, M. Mittelbronn, P. Burgard, et al., Multifactorial modulation of susceptibility to l-lysine in an animal model of glutaric aciduria type I, Biochim. Biophys. Acta (BBA) - Mol. Basis Dis. 1852 (2015) 768–777.
[60] P. Jafari, O. Braissant, P. Zavadakova, H. Henry, L. Bonafe, D. Ballhausen, Ammonium accumulation and cell death in a rat 3D brain cell model of glutaric aciduria type I, PLoS One 8 (2013), e53735, .
[61] V. Walker, Ammonia toxicity and its prevention in inherited defects of the urea cycle, Diabetes Obes. Metab. 11 (2009) 823–835.

[62] Y. Xu, Y. Yang, J. Ding, C. Li, iGlu-Lys: a predictor for lysine glutarylation through amino acid pair order features, IEEE Transac. Nanobiosci. 17 (2018) 394–401.
[63] M. Tan, C. Peng, K.A. Anderson, P. Chhoy, Z. Xie, L. Dai, et al., Lysine glutarylation is a protein posttranslational modification regulated by SIRT5, Cell Metab. 19 (2014) 605–617.
[64] J. Schmiesing, S. Storch, A.C. Dörfler, M. Schweizer, G. Makrypidi-Fraune, M. Thelen, et al., Disease-linked Glutarylation impairs function and interactions of mitochondrial proteins and contributes to mitochondrial heterogeneity, Cell Rep. 24 (2018) 2946–2956.
[65] W.J. Zinnanti, J. Lazovic, E.B. Wolpert, D.A. Antonetti, M.B. Smith, J.R. Connor, et al., A diet-induced mouse model for glutaric aciduria type I, Brain. 129 (2006) 899–910.
[66] S. Robel, S.C. Buckingham, J.L. Boni, S.L. Campbell, N.C. Danbolt, T. Riedemann, et al., Reactive astrogliosis causes the development of spontaneous seizures, J. Neurosci. 35 (2015) 3330–3345.
[67] J.E. Burda, A.M. Bernstein, M.V. Sofroniew, Astrocyte roles in traumatic brain injury, Exp. Neurol. 275 (Pt 3) (2016) 305–315.
[68] M. Pekny, M. Pekna, A. Messing, C. Steinhäuser, J.M. Lee, V. Parpura, et al., Astrocytes: a central element in neurological diseases, Acta Neuropathol. 131 (2016) 323–345.
[69] M. Humbert-Claude, D. Duc, D. Dwir, L. Thieren, J. Sandström von Tobel, C. Begka, et al., Tollip, an early regulator of the acute inflammatory response in the substantia nigra, J. Neuroinflammation 13 (2016) 303.
[70] S.I. Goodman, M.D. Norenberg, R.H. Shikes, D.J. Breslich, P.G. Moe, Glutaric aciduria: biochemical and morphologic considerations, J. Pediatr. 90 (1977) 746–750.
[71] S. Olivera-Bravo, C.A. Ribeiro, E. Isasi, E. Trías, G. Leipnitz, P. Díaz-Amarilla, et al., Striatal neuronal death mediated by astrocytes from the Gcdh−/− mouse model of glutaric acidemia type I, Hum. Mol. Genet. 24 (2015) 4504–4515.
[72] O. Braissant, P. Jafari, N. Remacle, H.P. Cudre-Cung, Do Vale Pereira S, Ballhausen D. Immunolocalization of glutaryl-CoA dehydrogenase (GCDH) in adult and embryonic rat brain and peripheral tissues, Neuroscience. 343 (2017) 355–363.
[73] M.V. Sofroniew, Astrogliosis, Cold Spring Harb. Perspect. Biol. 7 (2014) a020420.
[74] M. Nasser, H. Javaheri, Z. Fedorowicz, Z. Noorani, Carnitine supplementation for inborn errors of metabolism, The Cochrane Database of Systematic Reviews, 2009 , Cd006659.
[75] S.W. Sauer, S. Opp, A. Mahringer, M.M. Kamiński, C. Thiel, J.G. Okun, et al., Glutaric aciduria type I and methylmalonic aciduria: simulation of cerebral import and export of accumulating neurotoxic dicarboxylic acids in in vitro models of the blood-brain barrier and the choroid plexus, Biochim. Biophys. Acta 2010 (1802) 552–560.
[76] S. Kölker, S.W. Sauer, R.A. Surtees, J.V. Leonard, The aetiology of neurological complications of organic acidaemias–a role for the blood-brain barrier, J. Inherit. Metab. Dis. 29 (2006) 701–704 (discussion 5-6).
[77] J.M. Tarasoff-Conway, R.O. Carare, R.S. Osorio, L. Glodzik, T. Butler, E. Fieremans, et al., Clearance systems in the brain-implications for Alzheimer disease, Nat. Rev. Neurol. 11 (2015) 457–470.
[78] H. Benveniste, X. Liu, S. Koundal, S. Sanggaard, H. Lee, J. Wardlaw, The Glymphatic system and waste clearance with brain aging: a review, Gerontology. 65 (2019) 106–119.
[79] I. Suarez, G. Bodega, B. Fernandez, Glutamine synthetase in brain: effect of ammonia, Neurochem. Int. 41 (2002) 123–142.
[80] S. Kolker, G.F. Hoffmann, D.S. Schor, P. Feyh, L. Wagner, I. Jeffrey, et al., Glutaryl-CoA dehydrogenase deficiency: region-specific analysis of organic acids and acylcarnitines in post mortem brain predicts vulnerability of the putamen, Neuropediatrics. 34 (2003) 253–260.
[81] M. Wajner, S.I. Goodman, Disruption of mitochondrial homeostasis in organic acidurias: insights from human and animal studies, J. Bioenerg. Biomembr. 43 (2011) 31–38.
[82] B. Seminotti, A.U. Amaral, R.T. Ribeiro, M.D.N. Rodrigues, A.L. Colin-Gonzalez, G. Leipnitz, et al., Oxidative stress, disrupted energy metabolism, and altered signaling pathways in Glutaryl-CoA dehydrogenase knockout mice: potential implications of Quinolinic acid toxicity in the neuropathology of Glutaric Acidemia type I, Mol. Neurobiol. 53 (2016) 6459–6475.
[83] S.W. Sauer, J.G. Okun, M.A. Schwab, L.R. Crnic, G.F. Hoffmann, S.I. Goodman, et al., Bioenergetics in glutaryl-coenzyme a dehydrogenase deficiency: a role for glutaryl-coenzyme a, J. Biol. Chem. 280 (2005) 21830–21836.
[84] A.U. Amaral, B. Seminotti, J.C. da Silva, F.H. de Oliveira, R.T. Ribeiro, G. Leipnitz, et al., Acute lysine overload provokes marked striatum injury involving oxidative stress signaling pathways in glutaryl-CoA dehydrogenase deficient mice, Neurochem. Int. 129 (2019) 104467.
[85] A. Martínez Bermejo, I. Pascual Castroviejo, B. Merinero, Y. Campos, V. López Martín, J. Arcas, et al., Complex I and IV deficits in the mitochondrial respiratory chain in two siblings with type I glutaric aciduria, Neurologia (Barcelona, Spain) 9 (1994) 303–306.
[86] B. Ellenbroek, J. Youn, Rodent models in neuroscience research: is it a rat race? Dis. Model. Mech. 9 (2016) 1079–1087.